

Dr. Josep M^a Chimenos i Ribera
*Departament de Ciència de Materials i
Química Física*

Sr. Àlex Maldonado Alameda
*Departament de Ciència de Materials i
Química Física*



B Universitat de Barcelona

**Grau d'Enginyeria
de Materials**

Treball Final de Grau

**Synthesis and characterization of Alkali Activated Cements based
on Bottom Ash and Paval.**

**Síntesi i caracterització de Ciments Activats Alcalinament basats
en Escograva i Paval.**

Jofre Mañosa Bover

Juny 2018



Dos campus d'excel·lència internacional

B:KC Barcelona
Knowledge
Campus

HUB^c Health Universitat
de Barcelona
Campus

Aquesta obra esta subjecta a la llicència de:

Reconeixement–NoComercial-
SenseObraDerivada



<http://creativecommons.org/licenses/by-nc-nd/3.0/es/>

*It's the job that's never started as takes
longest to finish.*

J.R.R. Tolkien

En primer lloc el meu agraïment als meus tutors, el Dr. Josep Maria Chimenos i l'Àlex Maldonado per la seva ajuda i gran implicació en aquest projecte. Gràcies per tots els consells i recomanacions que m'heu fet tan en conceptes teòrics com en el procediment experimental durant el desenvolupament del projecte.

També agraeixo a tots els membres del grup de recerca DIOPMA que sempre m'han donat un cop de mà quan ho he necessitat.

Agraeixo a la meua família tot el suport que m'ha donat, especialment al meu pare per poder trobar temps sempre per ajudar-me i aconsellar-me, no només en aquest projecte sinó al durant tota la carrera.

Per últim el meu agraïment a l'Anna amb qui he compartit gran part del procediment experimental i ens hem ajudat mútuament al llarg de tot el projecte.

REPORT

CONTENTS

1.	SUMMARY	3
2.	RESUM	5
3.	INTRODUCTION	7
3.1	Alkali Activated Materials	8
3.2	AAC produced by industrial by-products and waste	11
3.3	Objectives	13
4.	EXPERIMENTAL PROCEDURE	15
4.1	Raw materials	15
4.2	Raw materials preparation	18
4.3	Sample preparation	22
4.4	Raw materials and samples tests	26
5.	RESULTS AND DISCUSSION	35
5.1	Raw materials	35
5.2	Test samples 1	41
5.3	Test samples 2	41
5.4	Test samples 3	42
5.5	Best formulation selection	47
5.6	Definitive samples	48
6.	CONCLUSIONS	55
7.	REFERENCES AND NOTES	57

8.	APPENDIX 1: GLOSSARY	63
9.	APPENDIX 2: ECONOMIC EVALUATION	65
10.	APPENDIX 3: RAW MATERIALS PSD	67
11.	APPENDIX 4: MASS AND VOLUME VARIATION	69
11.1	Test samples 3	69
11.2	Definitive samples	70
12.	APPENDIX 5: PAVAL MOISTURE DETERMINATION	71
13.	APPENDIX 6: LEACHING TEST RESULTS	73
14.	APPENDIX 7: XRD RESULTS	75
15.	APPENDIX 8: FTIR RESULTS	77
16.	APPENDIX 9: RAW MATERIALS SEM AND EDS	79
16.1	BA SEM images	79
16.2	BA EDS	80
16.3	Paval SEM images	83
16.4	Paval EDS	84
17.	APPENDIX 10: TEST SAMPLES 3 SEM	87
17.1	NaOH 2M samples	87
17.2	NaOH 4M samples	90
17.3	NaOH 6M samples	92
18.	APPENDIX 11: DEFINITIVE SAMPLE SEM, EDS AND QUANTITATIVE ANALYSIS	97
18.1	Definitive sample SEM images	97
18.2	Definitive samples EDS	98

1. SUMMARY

One of the most important challenges of European Union (EU) is to reduce the amount of municipal waste and industrial by-products generated since they are one of the main threats to the environment. For this reason, the valorisation of this waste and by-products has emerged, to produce compatible and viable products. If we focus on construction materials, some of these waste and by-products that have a large SiO_2 , Al_2O_3 and CaO content can be used to produce cements. Alkali Activated Cements (AAC) stands out as one of the best choices to produce this cements, since they can compete with Portland cements and they are also more sustainable.

The main purpose of this project is to synthesize and study AAC based in two by-products: municipal waste incineration bottom ash and Paval, an industrial by-product generated in aluminium production, by using as alkaline activators NaOH and Na_2SiO_3 .

The results obtained in this project demonstrate that with this two by-products it is possible to synthesize AAC, and that their mechanical properties are good enough to study them in more detail to make them a real alternative to Portland cements.

Different formulations have been considered by changing the proportions of this by-products and the alkali activators to determine which formulation gives rise to best results. It has been concluded that the AAC synthesized with bottom ash and 10% of Paval and activated with NaOH 6M are the formulations that give rise to better properties.

2. RESUM

En els darrers anys, un dels reptes més importants de la Unió Europea (EU) és el de reduir els residus sòlids urbans i industrials generats ja que són una de les principals amenaces pel medi ambient. Per això s'està impulsant la valorització d'aquests residus per fer-ne productes viables i compatibles. Centrant-nos en el camp de la construcció, alguns d'aquests residus que tenen elevat contingut en SiO_2 , Al_2O_3 i CaO es poden utilitzar per produir ciments. Un tipus de material que destaca en aquest camp són els Ciments Activats Alcalinament (AAC) ja que poden competir amb el ciment Portland i són molt més sostenibles.

Aquest projecte té com a objectiu principal la formació i l'estudi de AAC a partir de dos sub-productes: les escòries d'incineració de residus sòlids urbans i el Paval, un sub-producte generat en la producció d'alumini, utilitzant com a activadors alcalins NaOH i Na_2SiO_3 .

Els resultats obtinguts en el projecte demostren que efectivament amb aquests sub-productes es poden sintetitzar AAC, i que les seves propietats mecàniques són suficientment bones com per seguir-los estudiant i que arribin a ser una alternativa real als ciments Portland.

S'han dut a terme diferents formulacions variant les proporcions d'aquests sub-productes i els activadors alcalins per determinar quina era la que millors resultats dona. S'ha arribat a la conclusió que els AAC produïts amb les escòries i un 10 % de Paval, activats amb NaOH 6M són amb els que més bones propietats s'obtenen.

3. INTRODUCTION

In the present days, the most produced materials in the field of construction are steel and cement. If we focus in cement, it can be seen that recently, in year 2017, the global production of Portland cement and concrete was 4100 Mt, making it one of the largest manufactured material, just comparable with iron based materials [1].

Due to that huge amount of cement generated and to its current methods of processing, the construction sector is one of the most contaminating ones, either in gas emission and energetic consumption. In fact, Portland cement accounts for 2/3 of total energy production of non-metallic minerals [2]. Its production consumes on average between 4 to 5 GJ per tonne of Portland cement, mainly because of the high temperatures that have to be reached to produce clinker (about 1450°C) [3], [4], [2]. In terms of carbon dioxide (CO₂) expelling, for example, the production of one tonne of Portland cement releases approximately about 800 kg of CO₂ to the atmosphere. Every year more and more CO₂ is emitted, reaching the value of 32,5 gigatons in 2017, a value never documented before [5]. Only the Portland cement production contributes to this high CO₂ emitted value with between 5-8 % [6].

If contamination and energy consumption reduction is wanted, two options are possible. On the one hand, the manufacturing process could be changed, and on the other hand cement could be partly or mainly replaced by other material that satisfies the requirements of cement, which in addition, it must be eco-friendly. These two options lead to two possible solutions, either changing the cement production process or finding a new material that meets the mechanical requirements and being eco-friendly. The first solution is very complicated to carry out since all the fabrication methods are very standardized and defined, so it would be difficult to change them. Consequently, the only plausible choice is to replace cement by other material. A possible alternative to Portland cement is the family of alkali activated cements (AAC).

3.1 ALKALI ACTIVATED MATERIALS (AAM)

The AAM embrace any binder which derives from the reaction of an alkali metal source (usually in dissolution) with a powder shape precursor. This solid material can be a calcium silicate as in the conventional clinkers, or an aluminosilicate richer precursor such as metakaolin or some industrial by-products and waste like Fly Ash (FA) or metal slags. Regarding to the alkali source (activator), it could be any substance that fulfil a few main requirements:

- Provide alkaline or alkaline earth metal ions.
- Raise the pH of the reaction mixture.
- Accelerate the dissolution of the solid precursor.

The AAM are frequently named inorganic polymers or geopolymers, due to their formation process. However the term geopolymer is applicable only for the low-calcium and calcium-free AAM, those which are almost only aluminosilicates [6]. Nevertheless, due to the increasing popularity of these geopolymers in addition to other non-technical reasons, in many articles and publications the AAM will be named as geopolymers [4].

The introduction of the AAM in the construction sector should give rise to a significant reduction in the CO₂ emitted to the atmosphere [7]. Specifically, the reduction of CO₂ released (compared with Portland cement) estimated from a Life Cycle Analysis (LCA) is between 30-80 % [4]. It would also imply the reduction of approximately 43-59 % of the energy needs in the manufacture of AAC in comparison with Portland cement [3].

To get a complete understanding of what an AAM is, we should consider their generation. The formation of geopolymers is based mainly in five steps as shown in Figure 1 [8]:

- Dissolution of the solid particles by alkaline hydrolysis. Water is consumed.
- Speciation equilibria in the solution, such as silicates, aluminates and aluminosilicates.
- Gelation: At high pH, aluminosilicates dissolve very quickly generating a supersaturated solution, that will produce networks by condensation, called gels. During the process, water is released, but it stays in form of pores in the gel. The

time of this stage will highly depend on the reactants and the conditions in which it is carried out.

- Reorganization as the connectivity of the gel rises, giving rise to an aluminosilicate three-dimensional network.
- Polymerization, in which the nucleation and growth steps take place. First, the nuclei of the polymeric species are formed, and later these nuclei start to develop and grow. After that, there is a time in which the polymer gets harder.

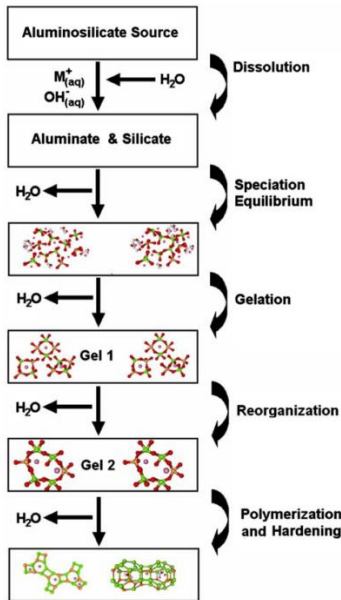


Figure 1: AAM formation

The structure of the gel is a three-dimensional network mostly made of silicate and aluminate tetrahedrons, which give rise to a negative charge in the aluminium tetrahedrons, considering that the aluminium ion is Al³⁺, while silicon ion is Si⁴⁺. This negative charge must be stabilized, and the metal cations provided by the alkaline solution will do this task. They will bond to the aluminosilicate network making the structure to be neutral. In spite that the structural distribution of molecules in AAM is difficult to determine, there are still some reports of it [9].

The properties of the geopolymer will depend on a lot of parameters: the reactants used (the activator solutions and precursors), the amount of these reactants, the Si/Al ratio, the porosity of the gel, the density, and many others.

About the general properties of the AAC, it must be said that all of them will be different for different types of AAC, and even in the same type of AAC, the properties can also change, depending for instance on the temperature at which the AAC has been obtained, the porosity, etc. Despite all these possible variations, this kind of materials are characterized by having a great resistance, especially if they work on compression, which makes them suitable to compete with Portland cements [10]. AAC show also superior resistance to chemical attack by aggressive aqueous solutions, compared to Portland cement, either acid solutions (i.e. solutions with SO_4^{2-} , Cl^-) or alkaline solutions [10]. AAC fire resistance is also higher than in Portland cements [10], [11], as well as lower permeability of water and chloride ions in moist conditions [11].

However, an important drawback in the AAC is that it is not guaranteed that they will present enough durability. While some authors state that the durability of this materials constitutes the main advantage over Portland cement others argue that it is an unproven issue [12]. The main benefit exhibited by these materials is found on the ecological side, since not only the CO_2 emitted, and the energy consumption is reduced, but also the AAC can be made from by-products or waste materials, that would contribute to make the material more sustainable.

The most important application of AAC is as a construction material, although it is difficult to apply because they have to compete with Portland cements that are commonly used nowadays and whose properties have been largely studied [13]. But this is not the only application, there are others that are worth mentioning. For instance, the ability of absorb heavy metals from a dissolution [14], applications related with its high fire resistance [15], or the retention of toxic waste inside their structure [13], along with many other applications, more or less investigated, but all of them very interesting to study.

3.2 AAC PRODUCED BY INDUSTRIAL BY-PRODUCTS AND WASTE

As already mentioned, AAC can be produced using several industrial by-products. The most common industrial by-products used to fabricate this kind of materials due to their abundance, is FA produced in power plants during the combustion of coal [16]. But other waste could also be used. Some of them are the Bottom Ash (BA) that come from the incineration of municipal solid waste, municipal waste incineration FA [17], lignite BA [18], blast furnace slag [19], palm oil fuel ash [20], waste ceramics [21] and many others that have high content in SiO_2 and Al_2O_3 mainly.

This study will focus on Municipal Solid Waste Incineration Bottom Ash (MSWI BA) since in the European countries the amount of municipal solid waste incinerated gets bigger every year [22], and approximately 80% of incineration residue is BA [23]. That means that every year the quantity of BA keeps increasing as well, considering that in Municipal Solid Waste Incineration for every ton of waste, about 180-250 kg of BA is produced [24]. Therefore, the use of these MSWI BA as a precursor for the AAC would be convenient because on the one hand the volume of CO_2 would be reduced compared with usual Portland Cements, and on the other hand these BA could be revalorised, because otherwise they are very difficult to treat, and it is challenging to find an application for them.

3.2.1 Bottom Ash

The MSWI BA are the part of municipal waste that do not burn in the incineration process and remains as a by-product at the end of the process. They are mostly constituted by glass, synthetic ceramics, mineral phases (SiO_2 , CaCO_3 , CaO), and partially metallic phases (steel, iron oxidized, aluminium, copper), although they can also contain unburned organic matter [23], [25]. As they embrace all kind of solid waste, these BA are a mixture of almost all chemical elements, being the most abundant silicon, calcium, aluminium, iron and sodium [24].

Several studies have been conducted to determine the chemical composition of these BA, and it has been concluded that the coarse fractions contain mainly synthetic ceramics (i.e. bricks, tiles, porcelain, concrete, etc...) and container glass (therefore more SiO_2). The finest fractions, have large amount of SiO_2 too and a lot of aluminium which is

necessary (in its oxide form) to form AAC, but the main problem is that they contain also heavy metals and soluble salts [26]. In consequence of that, to produce AAC from MSWI BA it is better to use only the coarser fractions, because there is more SiO_2 and the presence of heavy metals and soluble salts would complicate a lot the formation of AAC, obtaining a material environmental-unfriendly and with worst mechanical properties.

However, if the coarse fractions are chosen, a problem may emerge, because there may be not enough aluminium in this part of the BA, since it has been previously removed (usually by Eddy currents), and not enough aluminium oxide (Al_2O_3). This would complicate the formation of an AAC and an aluminium oxide source would be needed to compensate this deficiency in the precursor (BA). As aluminium oxide must be provided, an interesting idea would be using another by-product that contains high content of this material. A by-product that accomplishes this requirement is Paval.

3.2.2 Paval

Paval is a product that comes from secondary aluminium production and from the manufacture of primary aluminium. It is a part from the protecting slag that helps to avoid the oxidation of the aluminium as it melts [27]. These slags contain NaCl and KCl that have been added precisely as a flux to produce the protecting slag and hold the metal oxides. In order to recover these reactants, the slag is submerged into water to get the salts (NaCl and KCl) dissolved, and after recrystallizing, to be re-used again in the same process, closing the loop.

Paval is what remains after this process, the part that does not dissolve in water, so it can be recovered by filtering the solution. Paval has a high aluminium oxide content (66-75 %), and other oxides such as SiO_2 (4-12 %), MgO (20-25 %) or aluminium itself that has not been oxidized and it has passed to the slag from the melted material [27].

Although Paval has a high aluminium oxide content, it is difficult to treat because a very complicated and expensive refinement process is necessary. For this reason, most of Paval ends in landfill or it is used as a substitute of bauxite [28]. If it is wanted to be managed in landfill, it must be previously neutralized [29]. There are studies to find the best way to do neutralize Paval, by hydrolysing [30], and by mixing with cast [31]. Some Paval ends as a filler of construction, mixed with Portland [32], in shapes as bricks, asphalt

or others. In addition, efforts have been made to create calcium aluminate glasses [33], among other possible treatments.

The high aluminium oxide content of Paval makes it a good candidate as an aluminium oxide source to compensate the deficiency of this oxide in the coarser BA. Although this particular by-product has not been used to that purpose, it has been used as a filler in other applications, for instance to make cement from Portland clinker [34]. In AAC, other by-products have been used, for example red mud, which is a waste in Bayer process (aluminium oxide production) which contains mainly iron oxide, and aluminium and silicon oxide in less amount. It has been mixed with FA [35], metakaolin [36] or iron furnace slags [37].

The aspects of BA and Paval mentioned above suggest that AAC could be obtained by using these two residues.

3.3 OBJECTIVES

The main purpose of this project is to evaluate the use of BA and Paval to synthesize an AAC. Different proportions of raw materials are used and then evaluated to perform a complete analysis. Hence, the specific objectives are:

- To perform several tests to determine the reactivity of raw materials used, such as chemical attacks together with ICP-OES.
- To characterize the raw materials as well as all the AAC obtained with different techniques as FTIR, SEM, XRD, XRF, ICP-MS to have information about their composition and structure.
- To determine the mechanical properties of the AAC synthesized (flexural and compressive strength), as well as the porosity and density of the AAC.
- To choose the optimal formulation that give rise to a better AAC taking all the previous points into account and evaluating the influence of NaOH molarity and Paval content.

4. EXPERIMENTAL PROCEDURE

On this chapter the products used for the synthesis of an Alkali Activated Cement, the methodology used, and the characterization techniques will be presented. We will also describe the equipment utilized for that purpose.

4.1 RAW MATERIALS

4.1.1 Bottom Ash

MSWI BA used in this project was provided by the company *Valorización de Escorias de la Combustión, SA (VECSA)*. This product is a mixture of powder and coarse particles which contains the non-burned materials after the incineration process, such as glass, rocks, iron, aluminium, etc (Figure 2).



Figure 2: Bottom Ash

These BA are the result from the incineration of municipal waste in the incineration plant of *Servei d'Incineració de Residus Sòlids Urbans, SA (SIRUSA)*, located in Tarragona. After the incineration, these BA pass through a process of natural weathering for two to three months in which the BA are chemically stabilized to its subsequent commercialization.

From these Weathered Bottom Ash (WBA), only the coarser particles (coarser than 8mm) will be used in this project, and this fraction will be prepared as follows in next chapters, and as shown in Figure 3.

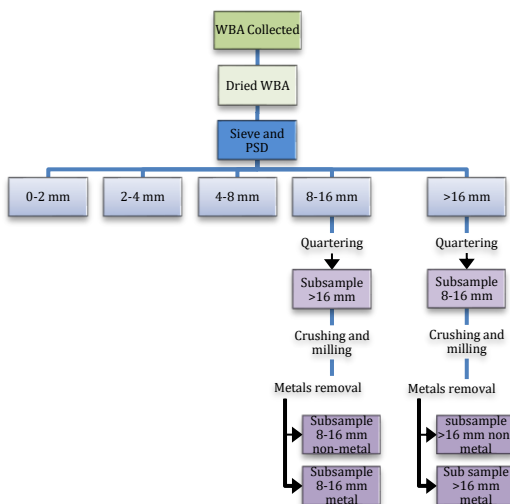


Figure 3: BA preparation scheme

4.1.2 Paval

Paval is a by-product from the secondary aluminium production. Paval used in this project was provided by Befesa, located in Valladolid. This product is mainly composed by Al_2O_3 and other metal oxides contained in the slag produced during secondary aluminium production.

Paval obtained in Befesa is the result of the process shown in Figure 4 [38]. This process consists on separating the salts used in secondary aluminium production from the oxides and from the pure aluminium contained in the slag. To do this separation process, first the slag is grinded and screened to separate the aluminium. After that process, the remaining material is mixed with water, this mixture is heated up and the salts will dissolve. They will be recovered by a crystallization process. The part that does not dissolve in water, are the metal oxides, that after being filtered and dried become the product named Paval [38].

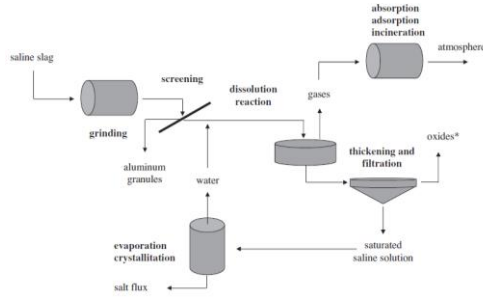


Figure 4: Scheme of the obtention of Paval in Befesa

Then the Paval must be prepared before using it to create the AAC, and it will be done as shown in Figure 5 (see next chapters).

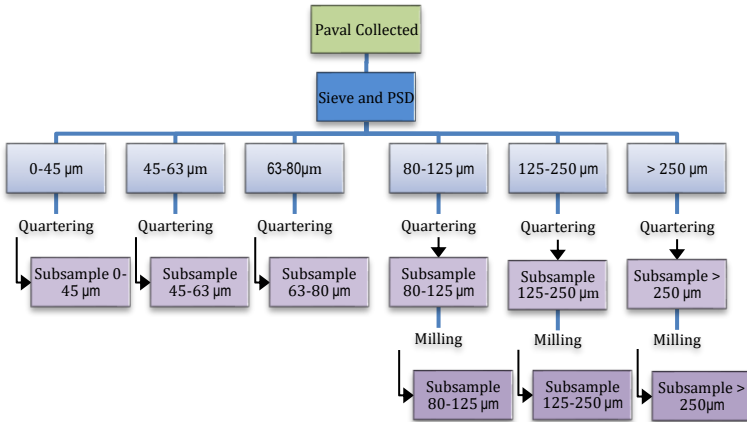


Figure 5: Paval preparation scheme

4.1.3 Sodium hydroxide

Sodium hydroxide (NaOH) is solid a chemical product obtained from the company VWR Chemicals, and it presents a purity of 98,5%. It was dissolved in water to do dissolutions of different molarity (M) to create the AAC.

4.1.4 Sodium silicate (Sodal)

Sodium silicate (Na_2SiO_3), also named Sodal, is a liquid chemical product provided by the company Scharlau, and which was used (along with NaOH) as liquid media to create the AAC.

4.2 RAW MATERIALS PREPARATION

4.2.1 BA drying

The WBA sample received contains a significant amount of water, and therefore it must be dried before being used. For that purpose, the sample it was placed in an oven at a temperature of 100 °C for 24 hours.

4.2.2 Raw materials sieving

As previously indicated, in this project only the 8 mm coarser fraction was used from the whole BA received, therefore, a sieving process must be made to separate this fraction.

By using a RETSCH vibratory sieve shaker AS 200 basic (Figure 6) and with sieves of 2 mm, 4mm, 8mm and 16mm, the whole sample of Bottom Ash was sieved, which resulted in 5 different particle size fractions: finer than 2mm, 2-4 mm, 4-8 mm, 8-16 mm and coarser than 16 mm. All these fractions were weighted, to compose a particle size distribution from the initial sample. After this process, the fraction coarser than 8 mm was separated.



Figure 6: RETSCH vibratory shaker AS 200 basic

Raw materials must have similar particle size to get a good mixing when the sample is prepared, so a particle size finer than 80 μm was used. To get that particle size, the samples of BA and Paval were grinded and sieved, but first, a particle size distribution of

the Paval sample initially received must be made, because the particle size of this material is fine, and hence some amount of the sample had passed the 80 μ m barrier.

Paval was sieved with sieves of 45 μ m, 63 μ m, 80 μ m, 125 μ m and 250 μ m. A particle size distribution was composed by the fractions finer than 45 μ m, 45-63 μ m, 63-80 μ m, 80-125 μ m, 125-250 μ m and coarser than 250 μ m. From these fractions, those coarser than 80 μ m were grinded later to get a particle size of maximum 80 μ m.

4.2.3 Raw materials quartering

To get a significant sub-sample of the whole Bottom Ash and Paval received, a quartering process must be made.

In the quartering process of the BA, the fraction previously separated (coarser than 8 mm) was extended on a flat surface in a circular shape it was and divided into 4 parts. Two of them were discarded and the other two parts were put together, as shown in Figure 7 [39]. The same process was repeated 3 times.

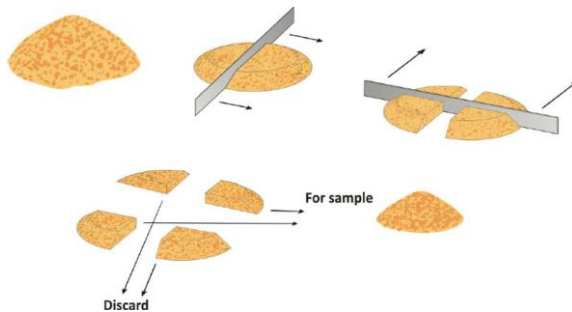


Figure 7: Quartering process

With Paval sample, the same process was made 4 times to get a significant amount to prepare the samples.

4.2.4 BA grinding

To get BA with a particle size of maximum 80 μ m, the sample must be grinded to reduce the size to prepare it for milling and to get powder of that particle size. Therefore, in a first step, a crusher with iron-chromium-nickel-vanadium jaws, shown in Figure 8 (a), was used to reduce the size of the coarser particles.

After this first grinding, a RETSCH model BB51 crusher was used, shown in Figure 8 (b). In this crusher the size at which the particles are crushed can be chosen, so the particle size was reduced first at a size of 4 mm, then at a size of 2,5 mm and finally at a size of 1,5 mm, since the equipment is not able to reduce the size directly to 1,5 mm.



Figure 8: Jaw crusher (a) RETSCH model BB51 crusher (b)

4.2.5 Raw materials milling

After being grinded, the raw materials must be milled to reach the size of $80\ \mu\text{m}$ to mix them and get a good mixture. To do that an eccentric ring mill RETSCH model RS100 was used shown in Figure 9 (a), with a steel bucket to avoid the bucket to react with the sample. The raw materials were distributed between the rings of the bucket shown in Figure 9 (b), with a total amount of 100 g maximum. When the material is completely distributed, the bucket is set inside the ring mill, and it is turned on with a velocity of 700 rpm for one minute. Then, the mill is stop and the bucket is left inside for five more minutes to avoid the finer particles to stick to the rings. After this time interval, the process is repeated two more times and then the bucket is extracted. Then, new amount of the raw materials is set in.

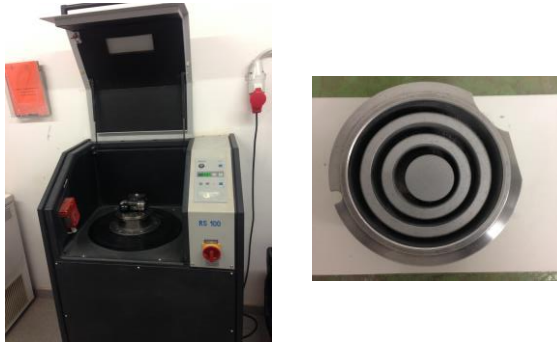


Figure 9: Eccentric ring mill RETSCH model RS100 (a) steel bucket (b)

4.2.6 Milled materials sieving

After all raw materials were milled, they must be sieved by using sieves of 80 μm and 250 μm . Therefore, fractions coarser than 250 μm , 80-250 μm and finer than 80 μm were obtained. Only the fraction with size finer than 80 μm will be kept. The other 2 fractions were treated to reduce their size again to less than 80 μm .

4.2.6 BA metal separation

In the fraction with particle size coarser than 250 μm there is a lot of aluminium pieces and some other metals. These particles must be taken away because in the mill they would only deform without reducing their size, thus making it difficult to reduce the size of the other particles and they might damage the equipment. In the fraction of 80-250 μm there are mainly iron particles (instead of aluminium), and they must be separated for the same reason explained above. This separation was done by using a magnet. The magnet was placed inside a plastic bag to avoid the particles to get attached to it, as shown in Figure 10 (a). This process was done to the fractions coarser than 250 μm and 80-250 μm . By using this method, most of the particles were separated (Figure 10), so the fractions of 80-250 μm and coarser than 250 μm were ready to be milled again.



Figure 10: Metal separation (a) Metal contained in BA (b)

The re-milled materials were sieved again with the same sieves (80 μm and 250 μm) and the part less than 80 μm was kept. The other part was discarded because it is considered as only metallic particles, (this is the main reason why it does not mill to the desired size).

4.3 SAMPLE PREPARATION

4.3.1 Sample preparation protocol

To prepare samples, similar procedure was always followed, in order to avoid experimental errors that would lead to different final properties of the AAC.

The first step is to weight BA and Paval previously prepared as stated in section 4.2. They were placed in a recipient, and manually mixed by using a spatula during approximately 30 seconds to get a homogeneous mixture. Apart from that, Sodal and NaOH were weighted too, following the desired L/S relation, and always with a ratio 80%-20% Sodal-NaOH. The two liquids were mixed in a separate recipient.

The liquids were stirred with an IKA® RW 16 Basic Low Viscosity Electronic Overhead Stirrer (Figure 11) during 30 seconds at the lowest velocity (number 1 in this device), and then the solid precursor was added bit by bit to this recipient. The time to add the solid vary depending on the amount of solid precursor used, because it cannot be added all at the same time if a good mixture is desired. In this stage, the stirrer was always fixed at the same velocity as it was in the previous step. Finally, to get a homogeneous mixture, the solution was mixed at a high velocity for one minute.



Figure 11: IKA RW 16 Basic Low Viscosity Electronic Overhead Stirrer

After that mixture, the slurry was poured to another recipient which was labelled with a name and weighted. It was covered with a cap (or placed in a hermetic box in the case of coarser samples). Once it was covered, it was slightly tapped on a flat surface 60 times to make air leave the slurry and reduce the creation of porosity. Afterwards it was left for four days covered. After this time period, it was uncovered and after three more days the sample was ready to take it out from the container. Then it stayed out of the recipient a certain period of time which completes a time period of 21 days since the sample was prepared. After these 21 days, the samples were ready to be tested.

Some samples had to be cut by using a diamond disc and then smoothed before mechanical tests are taken, because they had defects in the top and the bottom due to the container.

4.3.2 Preliminary test samples

4.3.2.1 Moisture and time determination (test samples 1)

A series of test samples were fabricated in order to determine the optimal waiting times of the sample into the container and also to elucidate whether moist or dry environments were the best suited conditions for the 21 days period.

To study these two parameters, first 10 samples of 10 g of solid precursor and 8 g of liquid (L/S relation 0,8) were prepared. It was observed that the slurry was too fluid, therefore 10 more samples were made, this time by using a 0,5 L/S relation (10 g of solid precursors and 5 of liquid). Five samples were placed into a box with containers filled with water to simulate a moist atmosphere as shown in Figure 12. The moisture inside and

outside the box was controlled with a datalogger testo 174H. The other five samples were settled inside a hermetic plastic bag and placed outside the box.



Figure 12: Moist atmosphere samples

Subsequently, the containers were uncovered at selected days in the range 1-5 days both in moist conditions and normal conditions. After that waiting period, samples were removed from the pot after 7 days since the samples were prepared. For the time left until 21 days, the samples were measured every 7 days and weighted every day. After these 21 days period since the samples were prepared, selected samples were studied qualitatively to decide which parameters give rise to better results.

To avoid false results due to other variables, the Paval content was the same in all the samples, 0,5 g of the total solid mass.

4.3.2.2 L/S relation (test samples 2)

To perform a complete study, the physical parameters were first modified and later the chemical parameters (those related with the gel formation) were also modified. The physical parameter studied was the L/S relation, and three different relations were tested. Having seen that the L/S relation of 0,5 was better than the 0,8 previously studied, the tests realized were 0,5 L/S, 0,4 L/S and 0,6 L/S. 3 samples were made and the one with better workability (not too much solid or too much fluid) was the selected sample.

As previously stated, in the first study only the physical parameters were modified, so Paval was not added to these test samples, because it would have modified the chemical parameters.

4.3.2.3 NaOH molarity and % of Paval (test samples 3)

Having determined the optimal physical parameters (L/S relation), NaOH M and % of Paval were next modified to study the effect of chemical parameters and to see how these two variations affect the gel formation.

To execute this research, samples of 30 g of solid precursor and 18 of liquid media (0,6 L/S relation) were prepared. In these samples the molarity was varied with values 2M, 4M and 6M, whereas the Paval content used was 0%, 1%, 5% and 10% as show in Table 1. Therefore 12 test samples were created (Figure 13), according to the previous studies (atmosphere, uncovering time and L/S relation).

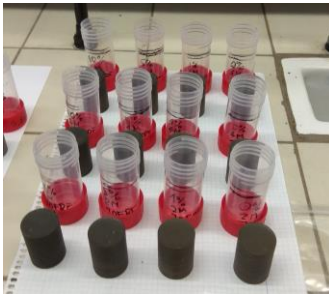


Figure 13: NaOH molarity and % Paval samples

The process described above was followed to prepare these 12 samples, with the following times: 30 s at velocity 1 to mix the two liquids, 1 min adding the solid precursor at velocity 1, 1 min of mixing the slurry at velocity 2, cover the container and slightly tap them 60 times on a flat surface, place them in a hermetic plastic bag.

Table 1: Test samples 3 formulations

2M				4M				6M			
0%	1%	5%	10%	0%	1%	5%	10%	0%	1%	5%	10%

4.3.3 Definitive samples

After that previous investigation, a molarity and an optimum Paval content was selected considering the results of the tests explained later in this work. With all the parameters defined, 3 samples of dimensions 4x4x16 cm³ were made (Figure 14). By

using a relation of proportionality between the mass and volume of the previous samples, we determined the required amount of solid and liquid to fill the 4x4x16 cm³ molds. The resulting masses of solid and liquid were 320 g and 192 g respectively.



Figure 14: Definitive samples

The preparation protocol followed was the same as before but changing the time to add the solid precursor to 4 min 30 s since the amount is larger. In this case, the slurry, once prepared, was poured in an expanded polystyrene mold, and to keep it hermetic, the mold was settled into a box, which was placed into a larger hermetic box. The times waited to uncover and unmold the samples were the same as in the previous tests: 4 and 7 days respectively.

4.4 RAW MATERIALS AND SAMPLES TESTS

4.4.1 Reactivity

4.4.1.1 Aluminium in Paval determination

This test (shown in Figure 15) is based on mixing paval with NaOH 1M to make the aluminium (in metal shape) react with the NaOH generating H₂ by following the reaction in Eq.1. The test was performed as explained in [26].



In these reactions, H₂ is released. That generates a volume change in a cylindrical tube full of water. By measuring this volume change, it is possible to determine the amount of aluminium in the sample tested.



Figure 15: Aluminium in Paval determination

4.4.1.2 Paval and BA chemical attacks

The amount of aluminium oxide and silicon oxide in paval and BA available to react to form the CASH or NASH gel, can be determined by chemically attacking the raw materials, and studying the resulting solution. We performed 4 attacks to the studied Paval and 2 in BA with 4 and 2 different solutions respectively as described in [40]. The first attack in both samples was done with a solution of 1% HF.

The attacks were done in a beaker, in which 100mL of the solution was poured with a later addition of 1 g of the sample. The solution remained in constant agitation using a magnetic stirrer. After 5 hours of agitation the solution was filtered using filter paper, and the solution was kept in a container. The solid remaining in the filter paper was also kept in another container.

The other three attacks were performed with a basic liquid: NaOH 2M, 4M and 8M (only 8M in BA). The process was the same, but with a temperature of 85°C. To reach this temperature, the beaker was placed in a water bath. To avoid gas leaving the solution, the beaker was covered with a cover, with water on its top, which promotes gas condensation (Figure 16). In these attacks, the resulting solutions were mixed with HNO₃ 68% to avoid precipitation.



Figure 16: Paval chemical attacks

All the tests were done in duplicate to obtain better results. The containers with the solution were kept in the fridge to avoid precipitation, until they were studied by Inductively Coupled Plasma – Optical Emission Spectrometry (ICP-OES).

4.4.2 Ambiental characterization

4.4.2.1 Leaching

A leaching test was made with an OVAN rotator R-HDE to determine the pH and the amount of Cl⁻ ions in raw materials, and to study its composition in Inductively Coupled Plasma – Mass Spectrometry (ICP-MS). The studied materials were Paval, BA without grinding and milling and BA after being grinded and milled. 50g of raw materials were placed in a cylindrical jar which was filled with deionized water up to a total mass of 500g, following the normative BS EN 12457 which stipule that a relation liquid-solid 10 l/kg is needed and that the material particles must be finer than 10 mm. It was sealed with a ribbed cover and leaching test was done for 24 hours at 40 rpm (see Figure 17).

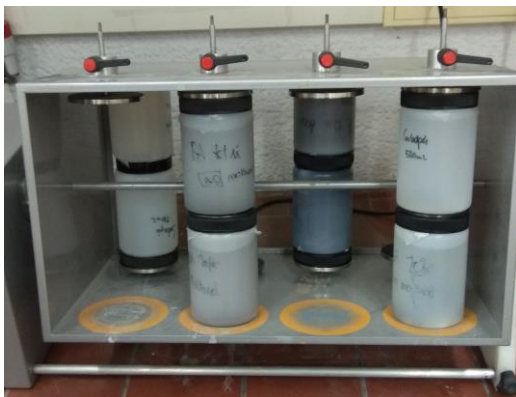


Figure 17: Leaching process

After 24 hours, the solution was filtered, first by using a filter paper, and then with a nitrocellulose filter of 45 μm , and two samples of 25 mL each were taken. In these two samples, pH was measured with a CRISON pH & ion-meter GLP 22. The same device working as a conductivity meter was used to measure the amount of chloride ions by adding buffer powder pillows (Figure 18).



Figure 18: pH and Cl ions measurement

Additionally, two samples of 10-15 mL approximately were taken from each jar, which were placed in a test tube, and a drop of HNO_3 68% was added to avoid precipitation. They were covered and analysed by ICP-MS.

The same test was done to the definitive samples once they are broken with the mechanical tests.

4.4.2.2 ICP-MS

ICP-MS was also used to determine the amount of specific metals (and some non-metals) present in the studied samples. The study was performed on the solutions prepared by leaching, as previously stated. The test was done at Centres Científics i Tecnològics de la UB (CCiTUB).

4.4.3 Physico-chemical characterization

4.4.3.1 Particle Size Distribution (PSD)

With this characterization technique, performed with a laser diffraction equipment (Beckman Coulter® LSTM 13 320) is possible to know the size distribution of the samples tested. In this project, BA and Paval grinded and milled were studied, to see if the size is similar. If the size is similar, it would mean that a better mixing will result when producing the AAC.

4.4.3.2 X-Ray Fluorescence (XRF)

An XRF test was performed to complement the XRD test. This test gives results of elements present in the sample studied.

4.4.3.3 X-Ray Diffraction (XRD)

XRD is a technique which enables to identify the different crystalline phases present in the studied samples by comparing the obtained diffraction patterns to the reference patterns. The samples were first grinded with an agate mortar and then encapsulated to be tested. The test will be performed with a diffractometer Siemens D-500 at CCiTUB.

This test is interesting to perform because by using this technique the crystallinity of the samples can also be known.

4.4.3.4 ICP-OES

ICP-OES is a characterization technique which gives an elemental quantitative analysis of the samples. In this technique, the samples previously obtained in chemical attacks were studied to find the Si and Al reactive in each different solution.

4.4.3.5 Fourier-Transform Infrared spectroscopy (FTIR)

To better determine the composition of the raw materials, an FTIR test was performed, in addition to other characterization techniques. In this test, a little amount of raw materials, in powder shape, was settled on the PerkinElmer FT-IR spectrometer Spectrum Two™ (Figure 19).



Figure 19: PerkinElmer FT-IR spectrometer Spectrum Two

FTIR test was also performed on test samples 3 and definitive samples. The samples were grinded with an agate mortar and then settled on the FTIR spectrometer in powder shape. The results were compared to data on handbooks to determine the composition of the samples.

4.4.3.4 Scanning Electron Microscopy (SEM)

The microstructure of the samples was studied with a FEI Quanta 200 Scanning Electron Microscope at CCiTUB (Figure 20). In SEM, images with different magnifications were taken using both secondary electrons (SE) and backscattered electrons (BSE).



Figure 20: SEM equipment

Furthermore, Energy Dispersive Spectrometry (EDS) test was also done, from which the elements contained in the sample were determined and also quantitized.

This assay was made to the raw materials and to the different samples (test samples 3 and definitive samples). Since samples in SEM must be conductive, a pervious coating process with carbon was made.

4.4.4 Mechanical tests

4.4.4.1 Compressive test

A compressive test is based on applying compressive forces to the sample until it breaks. The maximum force that the sample resists is known as compressive strength. The assay was made following the normative UNE-EN 196-1 with the equipment Incotecnic MULTI-R1, as shown in Figure 21 (a).

Compressive strength in MPa values were calculated as follows in Eq.2, where F(N) is the compressive force applied by the equipment and S(mm²) is the surface of the sample perpendicular to the force. The surface is different depending on the sample, for test samples it was πr^2 (mm²) whereas for definitive samples it was longitude multiplied by width, also in mm².

$$\sigma_c = \frac{F}{S} \quad (2)$$

This assay was performed to the properly prepared test samples to determine which of them have higher compressive strength and later also to the definitive samples.

4.4.4.2 Flexion test

This test is made with the same equipment as compressive test, but instead of applying the force to all the sample, it is exerted to only one section of the sample, as shown in Figure 21 (b). It can only be done if the sample is long, so only the definitive samples were tested in flexion test since test samples were cylindrical and not long enough. The result is the flexural strength of the material.

Flexural strength in MPa values were calculated as follows in Eq.3, where F(N) is the applied force, L(mm) is the distance between the supports, w(mm) is width and t(mm) is height.

$$\sigma_f = \frac{1,5 \cdot F \cdot L}{w \cdot t^2} \quad (3)$$

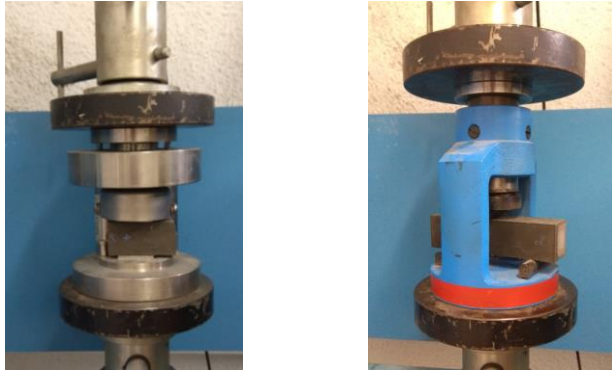


Figure 21: Compression test (a) Flexion test (b)

4.4.5 Physical tests

4.4.5.1 Porosity and density

The following protocol was followed to study the density and porosity in the samples investigated [41]. First, the samples were dried for 24 hours in an oven at 104°C. After drying, the samples were weighted (m_d) and then placed in a container and covered with a top that had a separatory funnel filled with water. Then vacuum was made by using a vacuum pump for 2 hours. After that time, water was poured inside without breaking the vacuum with the separatory funnel (Figure 22).



Figure 22: Porosity test

When the samples were completely covered by water, they were left in vacuum for 2 more hours and after that time, the pump was turned off and the samples were left inside the container with water until the following day to ensure that the water replace the air inside the pores.

The following day the samples were removed from the container and weighted first submerged in a container with water without touching any wall of the container (m_n), and

then they were dried using a wet drag to dry only the superficial water, and then they were weighted (m_s).

From these different masses (m_d , m_h , m_s), the porosity and the density of the samples can be computed as follows in Eq.4, Eq.5 and Eq.6.

$$\rho_a = \frac{m_d}{m_h} \quad (4)$$

$$\rho_r = \frac{m_d}{m_h - (m_s - m_d)} \quad (5)$$

$$p = \frac{m_s - m_d}{m_h} \cdot 100 \quad (6)$$

5. RESULTS AND DISCUSSION

In this chapter, the results of the different tests performed are presented and discussed to finally reach the conclusions of the project. First the results for the raw material tests are presented. Then we present the results for the prepared samples, in a chronological order (test samples 1, test samples 2, test samples 3 and definitive samples).

5.1 RAW MATERIALS

5.1.1 PSD

Two PSD were performed to raw materials: the first one to the BA received from VECSA, and the second one to the fraction of BA with particle size coarser than 8mm after being grinded, milled and sieved with an 80 μm sieve. For Paval the same procedure was followed.

The PSD graphics of raw materials untreated can be seen at Appendix 3: Raw materials PSD (Figure 48 and Figure 49). With regards to the test performed in the raw materials after being treated, it can be seen in Figure 23 that although the size distribution in BA is a little broader than in Paval, the curve in both materials match in the same sizes. This means that a good mixture was accomplished, because of the matching PSD and the fine particle size in both raw materials, which make the reactivity of the particles increase.

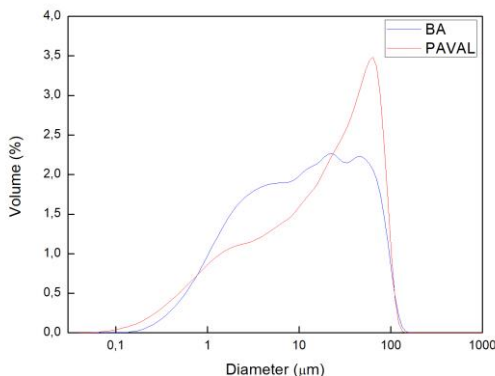


Figure 23: PSD for BA and PAVAL

5.1.2 Aluminium in Paval determination

The amount of aluminium in Paval was studied in Paval with particle size finer than 80 μm and also in Paval with particle size coarser than 80 μm . As shown in Table 2, the amount of metallic aluminium is different for the two tests. This difference is due to the fact that metallic aluminium is very ductile, and it deforms but it does not break in the ring mill, therefore the amount of Al in coarser particle size Paval is larger. This Al content is too large to the complete the test, because the volume of H_2 generated is too large. Therefore, the results were invalid because the volume change due to the metallic aluminium have place in less than 20 minutes instead of 4 hours (the time stipulated in the test [26]). To circumvent this error the test was performed with 1g of Paval instead of 5g, although due to the small amount the results may not be representative.

Table 2: Aluminium content in Paval

Sample	m Paval (g)	% Aluminium
Paval (<80 μm)	4,99	2,12
Paval (<80 μm)	4,99	2,27
Paval (>80 μm)	1,00	9,90

For the samples with particle size finer than 80 μm , the amount of aluminium is low. A higher Al content would increase the porosity in the samples would increase, since metallic aluminium reacts with NaOH forming H_2 which would remain trapped inside the sample.

5.1.3 Chemical attacks

5.1.3.1 BA chemical attacks

In BA the chemical attacks were performed as described in 4.4.1.2. In these attacks, the total availability of SiO_2 and Al_2O_3 is determined by the HF attack [40] (Figure 24). The availability of these reactants in the AAC formation depends on the M of the NaOH. The availability gets higher as M increases. The % of SiO_2 and Al_2O_3 in NaOH 8M attack is lower than in HF attack because in the NaOH attacks not all the % of SiO_2 and Al_2O_3 reacts. After performing the attacks, it was observed that the samples with NaOH 8M were too porous, so new molarities were chosen, 2M, 4M and 6M, expecting better results in 6M samples due to a higher amount of SiO_2 and Al_2O_3 available.

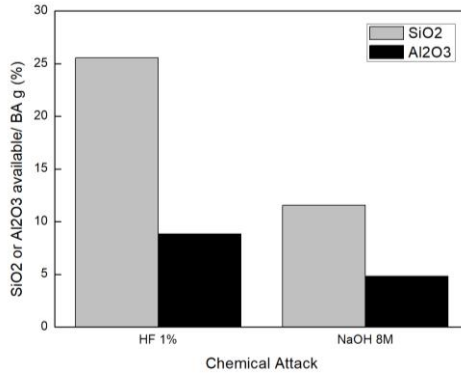


Figure 24: BA chemical attacks

5.1.3.2 Paval chemical attacks

The attacks in Paval were performed to determine if there is a high Al₂O₃ content, as reported in literature, and if the Al₂O₃ would react in alkaline media. It can be observed in Figure 25 that the amount of Al₂O₃ is high for the 4 different attacks, and therefore Paval will be a good Al₂O₃ source to compensate the lack of this oxide in the BA with particle size coarser than 8 mm. The largest value is reached in NaOH 2M. Although the amount of SiO₂ is low in Paval, it is irrelevant since SiO₂ is provided by BA.

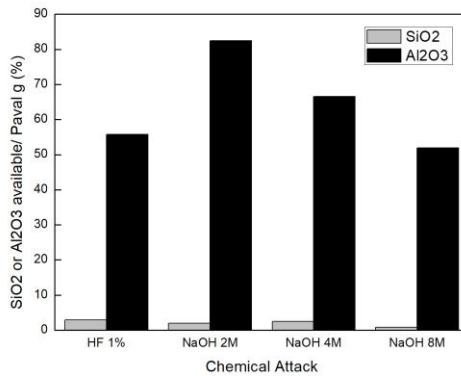


Figure 25: Paval chemical attacks

5.1.4 Leaching test

Leaching test was performed to determine the amount of hazardous elements in the raw materials and to compare the results with the prepared AAC. In the results obtained with ICP-MS presented in Table 13 (in Appendix 6: Leaching test results) it can be observed that the elements are below the hazardous limits except for Sb in Paval (according to the limit values (mg/kg) for compliance leaching test using BS EN 12457 [42]).

5.1.5 XRF

XRF test was performed to determine the composition of BA, and the results are shown in Table 3. As stated in previous chapters, the main elements are Si, Ca and Al. It can also be observed that there is a Loss on Ignition (LOI) of 5,4%, which could be due to the carbonates and hydrated phases in BA.

Table 3: XRF BA

Components	Fe ₂ O ₃	CaO	SiO ₂	Al ₂ O ₃	Na ₂ O	MgO	LOI rel (%)
Percentage (%)	4,00	14,31	56,87	8,26	6,52	2,42	5,40

5.1.6 XRD

XRD test was made to complement XRF to identify the crystalline phases in raw materials. This technique has a detection limit of 3% (it detects only phases more abundant than 3%) and if the analysed material is amorphous, this limit % increases. In both materials, the main crystalline phases were detected by using the software X'Pert HighScore, and the results and the graphs are shown in Figure 26. It can be observed that the composition results of BA match the results of the XRF test since we find mainly Si and Ca, and some minority phases which also match the elements in XRF (Al, Na...). While Paval has a straight background, BA have a broad hump in 15-30° (2θ) which is because the sample is partly amorphous [43], [44]. It is beneficial since the amorphous part is mainly aluminosilicates, the part that forms the gel.

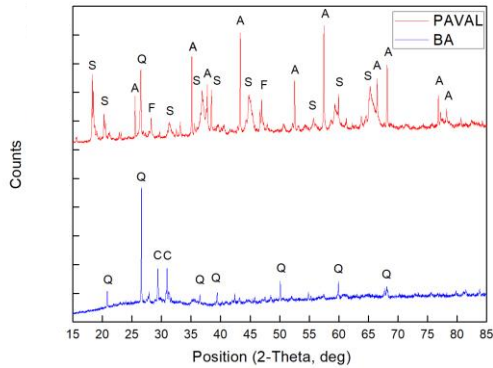


Figure 26: XRD patterns of BA and Paval. Q= quartz; C= calcite; A= aluminium oxide; S= spinel ($MgAl_2O_4$); F= fluorite

5.1.7 FTIR

We used FTIR to find the main motion of bonds in raw materials, to also characterise the raw materials and to compare the results with the results of the produced AAC. In BA pattern we can observe two bands, one at 1433.98 cm^{-1} which corresponds to a carbonate (probably $CaCO_3$) and one at 983.56 cm^{-1} which is due to Si-O-Si asymmetric stretching vibrations. There is also a shoulder at approximately 877 cm^{-1} which is due to the presence of quartz [45]. In Paval, we can see bands at 971.19 cm^{-1} and 503.17 cm^{-1} which are due to the phase $\alpha\text{-Al}_2\text{O}_3$ and to Al-O stretching respectively (Figure 27) [46].

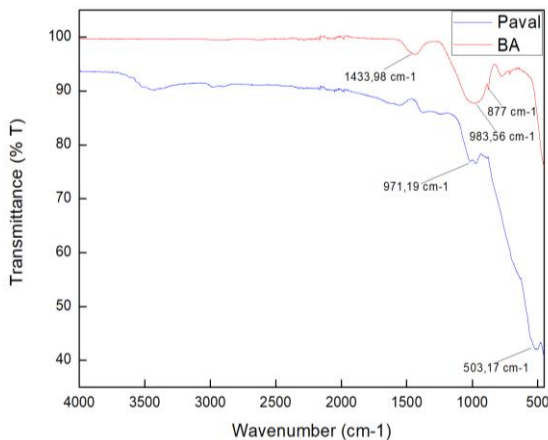


Figure 27: BA and Paval FTIR

5.1.8 SEM

The large heterogeneity in particle sizes in BA is observed by SEM image shown in Figure 28 (a). Figure 28 (b) indicates the spots where EDS test has been performed. Other SEM images and EDS graphics are included in Appendix 9: Raw materials SEM and EDS. Table 4 shows the heterogeneity in the composition of the sample.

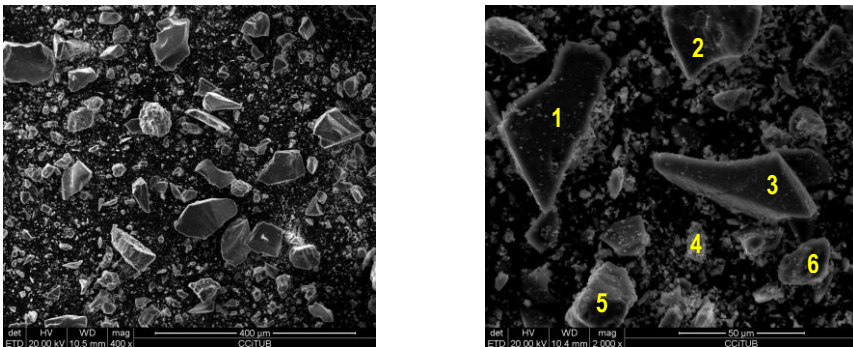


Figure 28: BA 400x (a) BA 2000x EDS spots (b)

Table 4: EDS spots composition in BA

SPOT	Composition
Spot 1	Si, O
Spot 2	Si, Al
Spot 3	Si, Ca, K
Spot 4	Si, Mg, O
Spot 5	Al, Si, O
Spot 6	Al, O

Figure 29 (a) shows Paval particles with different sizes in an 400x image, while Figure 29 (b) shows the spots where EDS test has been performed (see Appendix 9: Raw materials SEM and EDS). The composition corresponding to these spots are compiled in Table 5. Only the 2 spots shown in Table 5 have been studied in detail because the rest of particles in this image had the same composition, aluminium oxide or metallic aluminium.

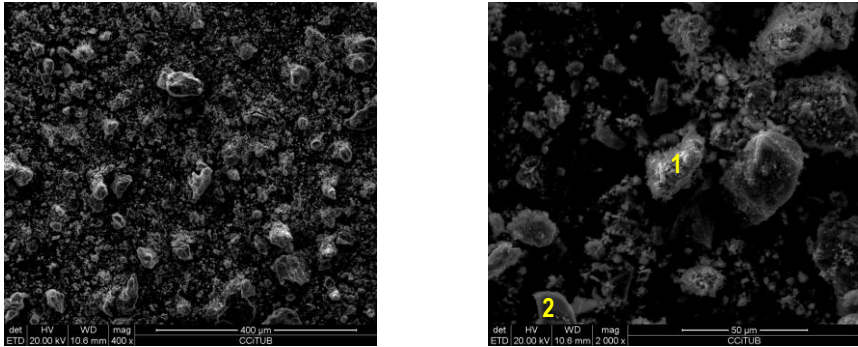


Figure 29: Paval 400x (a) Paval 2000x EDS spots (b)

Table 5: EDS spots composition in Paval

Spot	Composition
Spot 1	Al, O
Spot 2	Al

5.2 TEST SAMPLES 1

Test samples 1 were studied qualitatively. The first observation was that samples in moist atmosphere needed more time, because they were wet after two weeks placed inside the moisture box. Therefore, these samples were discarded. We also realized that the samples uncovered after one, two and three days presented unequal volume contraction (more contraction on the top and less in the bottom), changing the shape of the sample, therefore they were also discarded. Finally, among the samples uncovered after 4 and 5 days, the first was chosen because it was more consistent than the other.

5.3 TEST SAMPLES 2

As previously stated in chapter 4.3.2.2, test samples 2 were only prepared to study the workability of the slurry with different L/S relation. With a spatula the sample was mixed to determine if it was either fluid and viscous enough. 0,4L/S and 0,5 L/S were

found to be too viscous, and 0,6 L/S was not too fluid. Hence, 0,6 L/S relation was chosen to prepare the following samples.

5.4 TEST SAMPLES 3

5.4.1 XRD

To study in detail the changes in the pattern due to the Paval %, one sample with 0% of Paval and one sample with 10 % of Paval have been analysed with the software X'Pert HighScore (Figure 30). Furthermore, a graph of different molarities always with the same % of Paval (10%) has been done to study in detail the changes due to the molarity (Figure 31).

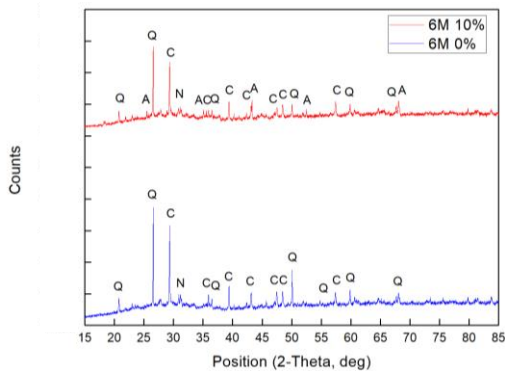


Figure 30: XRD patterns of samples with 0% and 10% of Paval. Q= quartz; C= calcite; A= aluminium oxide; N= Na and Ca aluminosilicates

When Paval % is changed some peaks increase their intensity and some additional peaks are detected. This new peaks are due to the addition of aluminium oxide (Al_2O_3), and because of this addition, the relative amount of quartz and calcite decreases (less intensity in some peaks of these phases). Furthermore, these samples give rise to new minority crystalline and amorphous phases that were not in raw materials (mainly aluminosilicates).

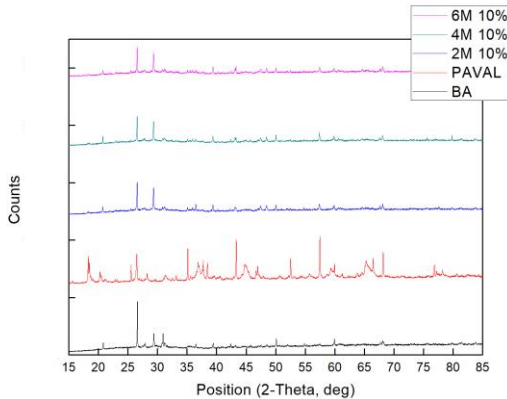


Figure 31: XRD patterns of samples with different molarities and 10% of Paval

It can be seen that the pattern stays almost independent of molarity, so all samples will exhibit the same phases (with possible small variations). The patterns corresponding to the other samples are plotted in Appendix 7: XRD results.

5.4.2 FTIR

In FTIR graphics, all the NaOH 6M patterns were plotted, and all the 10% of Paval were plotted. The rest of the FTIR graphs can be found at Appendix 8: FTIR results. In Figure 32 it can be observed that by changing the Paval content the bands get more intense as % increases. In 3000 cm^{-1} there are bands that appear in some formulations which are not from raw materials or the AAC geopolymer. They could be due to ethanol used to clean the equipment. If we compare the samples with BA there is a displacement of the bands, which is due to the gel formation.

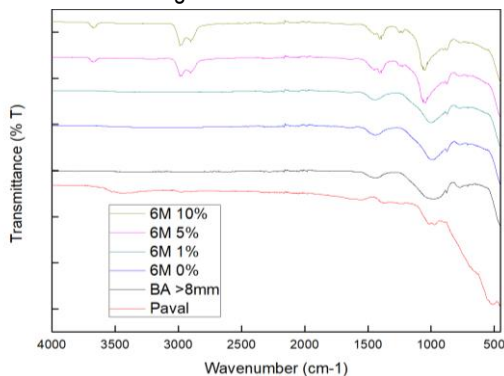


Figure 32: FTIR of NaOH 6M test samples 3

In regard to molarity contribution, it can be seen in Figure 33 that by depending on the NaOH molarity used the characteristic bands will change. In 2M the bands are very intense, while in 6M the bands have decreased and in 4M the main bands decrease their intensity and some bands even disappear. It can be due to a not complete reaction of the raw materials.

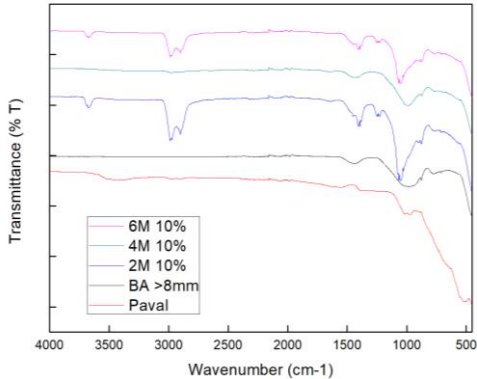


Figure 33: FTIR of 10% of Paval test samples 3

5.4.3 SEM

In this test, also images of NaOH 6M and 10% of Paval will be compared, to see which formulation is more cohesive, and have less defects. Other SEM images can be seen in Appendix 10: test samples 3 SEM. By looking at the images of 6M and changing the Paval %, it can be observed that in Figure 34 (b) and Figure 35 (a) the cracks in the sample are much larger than in the other two. If Figure 34 (a) Figure 35 (b) are compared, they look similar, but in the sample with 10% of Paval there is more cohesion.

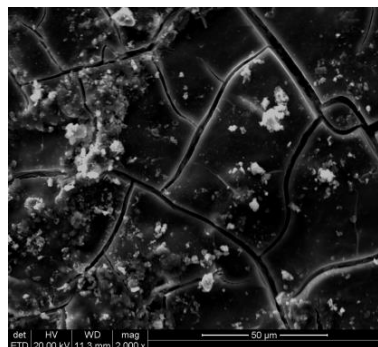
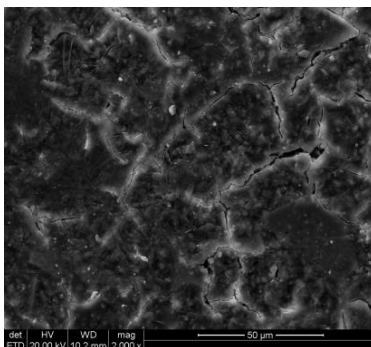


Figure 34: 0% 6M ETD 2000x (a) 1% 6M ETD 2000x (b)

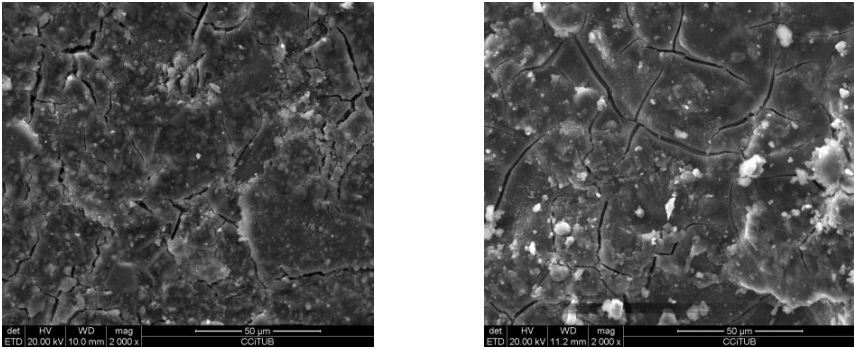


Figure 35: 5% 6M ETD 2000x (a) 10% 6M ETD 2000x (b)

If we focus in molarity, Figure 36 (b) presents large cracks which will cause problems in mechanical behaviour, so this sample is discarded. Figure 35 (b) and Figure 36 (a) look very similar, so we study the same sample but with 400x. It is observed that Figure 37 (b) presents better cohesion than the sample in Figure 37 (a).

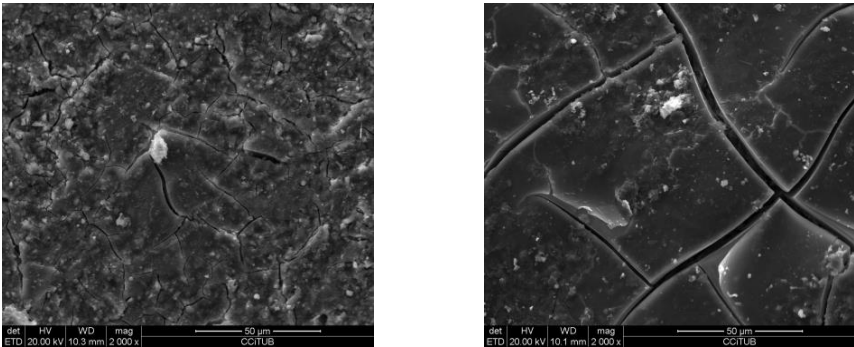


Figure 36: 10% 2 M ETD 2000x (a) 10% 4M ETD 2000x (b)

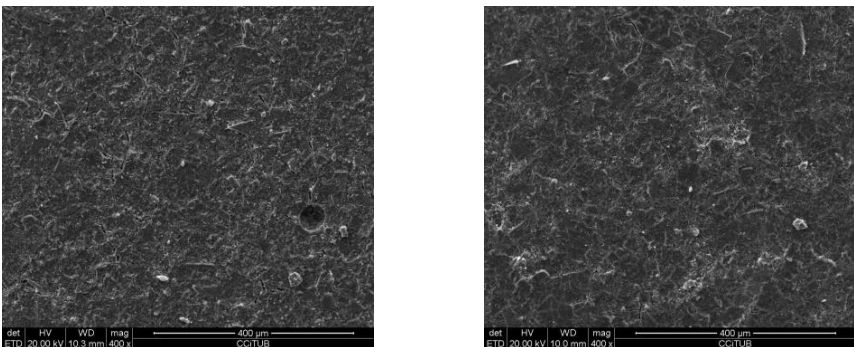


Figure 37: 10% 2M ETD 400x (a) 10% 6M ETD 400x (b)

5.4.4 Compressive test

In compressive test the data for compressive stress (MPa) are obtained by dividing the applied force by the cross-section of each sample. Results are shown in Figure 38. It must be mentioned that sample 5% 6M had a crack on the surface, and probably for this reason it cracked with a lower compressive stress applied.

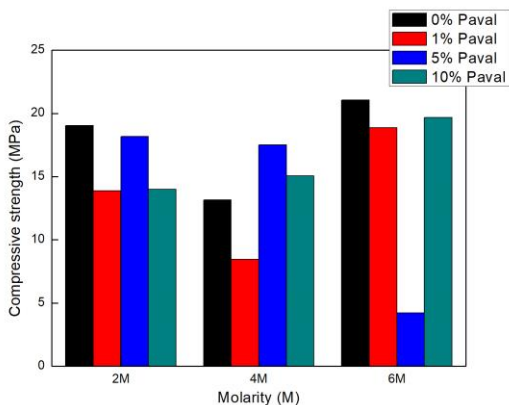


Figure 38: Compressive strength of test samples 3 by molarity and % of Paval

It can be concluded that the samples with higher compressive strength in general are the samples with NaOH 6M.

5.4.5 Porosity and density

In Figure 39 we plot the experimental values of apparent density and relative density calculated with the methodology explained in section 4.4.5.1 and apparent density calculated dividing mass by volume. In Figure 40 we plot porosity calculated with the methodology explained in section 4.4.5.1.

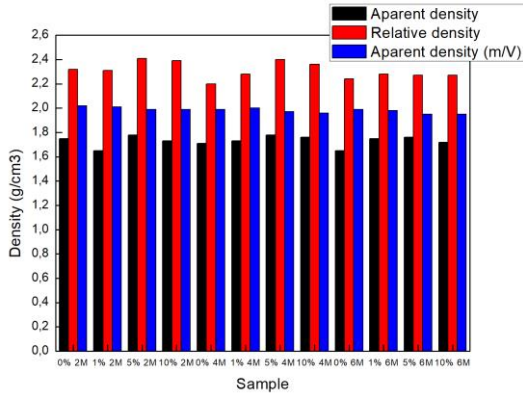


Figure 39: Density of test samples 3

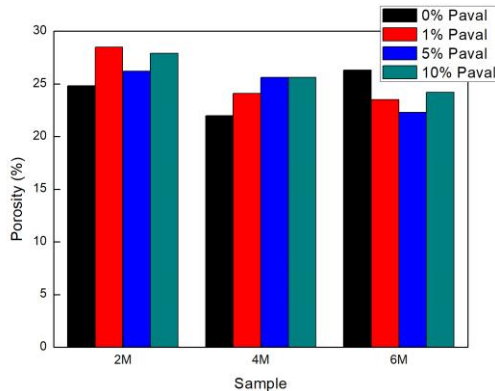


Figure 40: Porosity of test samples 3 by molarity and % of Paval

Although NaOH 2M samples seem to be more porous than the 4M and 6M, the results may not be conclusive.

5.5 BEST FORMULATION SELECTION

To select the optimal formulation to prepare the definitive samples, all the results presented before were considered. SEM images show that the formulation that presents better cohesion is 10% 6M. Furthermore, this same sample is the second with better compressive strength, only below the 0% 6M sample. Although the results in porosity test are not the best, the porosity of this sample is not high.

It has also been stated in section 5.1.3 that with higher molarity, SiO₂ availability will increase and that by adding Paval to BA, the amount of Al₂O₃ will also increase. This will help to create the gel (mainly aluminosilicates) required to form the AAC, so it means that the samples with higher Paval content and higher molarity should create more gel.

Due to all these reasons, the optimal formulation is 10% of Paval and NaOH 6M, so the definitive samples will be made with this formulation.

5.6 DEFINITIVE SAMPLES

5.6.1 Leaching test

The procedure of leaching test in definitive samples is the same as in the leaching test of raw materials. The leachates are analysed with ICP-MS to find the amount of hazardous materials and the results of the final samples are compared the results in raw materials. The normative BS EN 12457 stipulates that the particle size must be lower than 10 mm, so the sample must be crushed and sieved to accomplish this size requirement. The results represented are an average for the 3 samples studied.

Table 6: Definitive sample ICP-MS leaching test results

	Zn (mg/kg)	Pb (mg/kg)	Ni (mg/kg)	Cr (mg/kg)	Cu (mg/kg)	Ba (mg/kg)
Average	2,32	0,81	0,12	1,02	2,28	0,35
Inert limit	4	0,5	0,4	0,5	2	20
Non-hazardous	50	10	10	10	50	100
Hazardous limit	200	50	40	70	100	300

	As (mg/kg)	Cd (mg/kg)	Sb (mg/kg)	Mo (mg/kg)	Hg (mg/kg)
Average	1,54	0,01	2,62	0,96	0,24
Inert limit	0,5	0,04	0,06	0,5	0,01
Non-hazardous	2	1	0,7	10	0,2
Hazardous limit	25	5	5	30	2

The results listed in Table 6 are higher than in raw materials (Table 13) as the high pH of the solution used to synthesize the AAC activates heavy metals. However, the only hazardous element is Sb.

It must be mentioned that all the results listed would be lower if the sample had not been crushed, because cement encapsulates hazardous elements. However, to follow the normative it had to be crushed. It should also be noticed that although the same procedure has been followed for the three samples, results from leaching tests are not identical among the samples because of the heterogeneity of the raw material used.

5.6.2 XRD

For the definitive formulations, a representative sample has been analysed with the software X'Pert HighScore to find the most abundant phases (Figure 41). Compared to the previous sample with the same formulation it is observed that both patterns almost perfectly match but some peaks have slightly different height. This is because the relative amount of some phases has changed or could be due to experimental error.

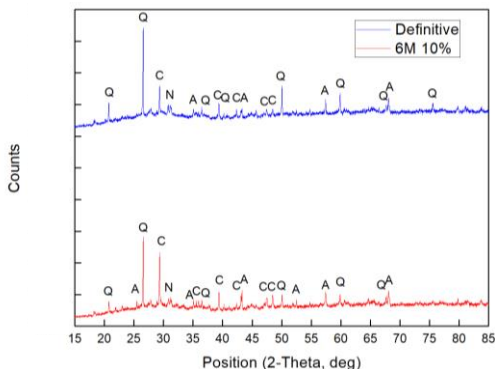


Figure 41: XRD patterns of 6M 10% sample and definitive sample

5.6.3 FTIR

We have compared FTIR data for the 10% 6M sample with the definitive sample. Analysis of the bands of this AAC is shown in Figure 42. In definitive sample we detect a broad band in $3328,76\text{ cm}^{-1}$ which corresponds to O-H stretching [47]. The band in $1418,24\text{ cm}^{-1}$ is due to the presence of a carbonate (Na_2CO_3 or CaCO_3) [45], and the peak at $983,51\text{ cm}^{-1}$ is due to Si-O-Si and Al-O-Si stretching [48]. In the 6M 10 % sample, the bands at $1050,33\text{ cm}^{-1}$ and $1394,09\text{ cm}^{-1}$ are Si-O-Si and Al-O-Si stretching and carbonate presence respectively. The broad and small peak in $3675,56\text{ cm}^{-1}$ is due to O-H stretching. Bands in $2901,19\text{ cm}^{-1}$ and $2987,99\text{ cm}^{-1}$ are not from raw materials or the AAC that could be due to the ethanol used to clean the equipment.

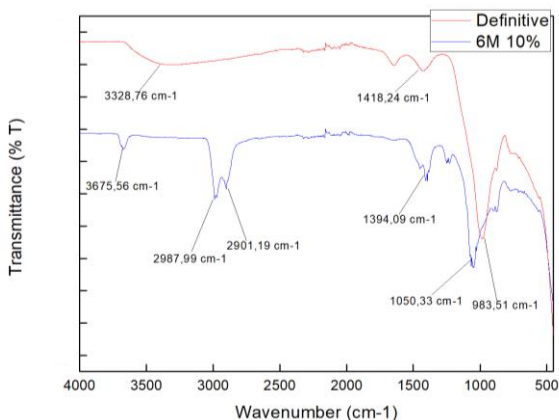


Figure 42: FTIR 6M 10% sample and definitive sample

5.6.4 SEM

SEM tests have been performed at 400x and 2000x (Figure 43 (a) and Figure 43 (b)). We have also studied selected spots with EDS (Figure 43 (b)) and the elements found are listed in Table 7. In Appendix 11: Definitive sample SEM, EDS and quantitative analysis we can see other SEM images and we detail the quantitative test with EDS in each spot, which provides the amount of each element in the spot.

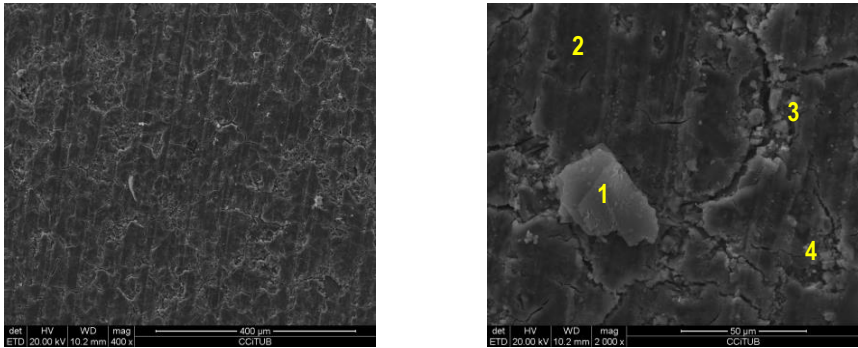


Figure 43: Definitive sample ETD 400x (a) Definitive sample ETD spots 2000x (b)

Table 7: EDS spots composition in definitive sample

Spot	Composition
Spot 1	C, Si
Spot 2	Si, Ca
Spot 3	Si, Ca, Na
Spot 4	Si, Al

Figure 43 (a) and Figure 43 (b) show that the cohesion in definitive sample is almost perfect, although it has some cracks. There are parallel bands due to the cut of the sample with the diamond disk. The high amount of C found in spot 1, is because this particle is probably a particle remaining from the carbon coating done to the sample to make it conductive.

5.6.5 Compressive test

A flexion test has been first performed on these samples (see 5.6.6) in which the samples have been broken in two parts. Then, a compression test has been made with each part of the samples. The results shown in Figure 44 show that the compressive strength is much lower than in test samples 3. It is due to the shape of test samples 3, which gives rise to better compressive strength.

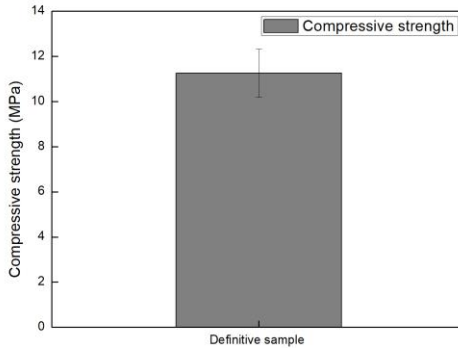


Figure 44: Definitive samples compressive strength

The results show that the values of compressive strength are almost the same for the three samples studied (low error), so their structure and shape must be very similar.

5.6.6 Flexion test

The results of flexion test are not as relevant as the compressive test results, but the test is representative. In Figure 45 it can be seen that the results in different samples coincide, so their structure and shape will be very similar.

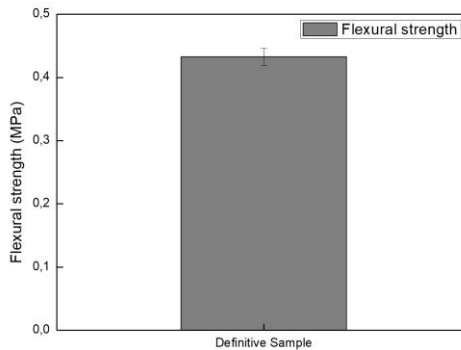


Figure 45: Flexural strength of definitive samples

5.6.7 Porosity and density

Porosity test was also performed to each definitive sample, to determine if the porosity was similar to the porosity in previous samples. If we compare the results in Figure 46 and in Figure 39, we observe that density is similar and there is a slight increase in density for definitive samples. If we compare Figure 47 and Figure 40 we observe that also porosity is similar and there is a decrease in porosity for the definitive samples, according to the decrease in density. These variations should give rise to better mechanical properties.

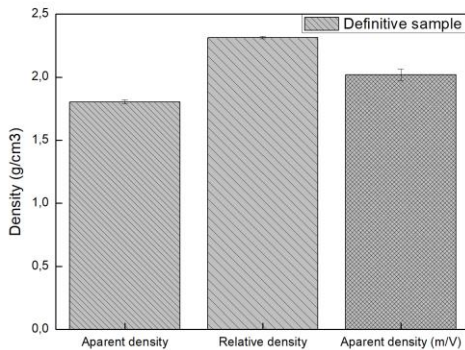


Figure 46: Density of definitive samples

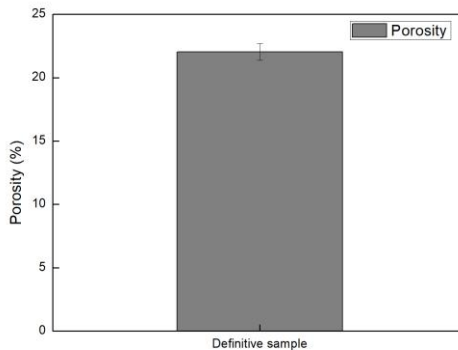


Figure 47: Porosity of definitive samples

6. CONCLUSIONS

The main conclusions are as follows:

It is possible to synthesize AAC based on BA (with coarse particle size) and Paval. This means that these by-products can be revalorised.

Physicochemical characterization shows that in AAC there is a large fraction of amorphous material, and that the main crystalline phases still are SiO_2 , CaCO_3 and Al_2O_3 (this last only in AAC with Paval) after the alkaline activation. SEM images show the geopolymer that enhances the particles and giving the material more cohesion and thus better properties.

These results together with mechanical properties give rise to the optimal formulation which is 0,6 L/S ratio with NaOH 6M and 10% of Paval. It has been observed that Paval does not improve mechanical properties despite its high Al_2O_3 content. Mechanical properties obtained allow the possibility to use these cements in construction field.

In regard to ambiental characterization, it has been observed that when the cements are activated, the content of heavy metals increase compared to raw materials. Previous treatment could be done to WBA to decrease this heavy metals content.

In future work there are several possibilities to new research:

- To study how curing time influence mechanical properties since in this project only samples with 21 days of curing have been studied.
- To synthesize samples in moist conditions to determine how moisture modifies the properties of the AAC.
- To change the methodology of sample preparation. First Paval can be mixed with NaOH to make the aluminium react before mixing Paval with BA. With this process H_2 generated by metallic aluminium will be released and will not create porosity. It can be studied if porosity can be reduced by applying this procedure.

7. REFERENCES AND NOTES

- [1] "Cement production globally and in the U.S. from 2010 to 2017 (in million metric tons)." [Online]. Available: <https://www.statista.com/statistics/219343/cement-production-worldwide/>. [Accessed: 15-Mar-2018].
- [2] M. Taylor, C. Tam, and D. Gielen, "Energy Efficiency and CO₂ Emissions from the Global Cement Industry," *IEA-WBCSD Cem. Energy Effic. Ind. Work.*, no. September, 2006.
- [3] J. Davidovits, "Geopolymer cement," no. 0, pp. 1–11, 2013.
- [4] J. L. Provis and J. S. J. van Deventer, *Alkali Activated Materials: State-of-the-Art Report, RILEM TC 224-AAM*. Springer Netherlands, 2013.
- [5] "Global Energy & CO₂ Status Report." [Online]. Available: <http://www.iea.org/geco/emissions/>. [Accessed: 22-Mar-2018].
- [6] J. L. Provis and J. S. J. Van Deventer, *Geopolymers : structure, processing, properties and industrial applications*. Woodhead, 2009.
- [7] E. Gartner, "Industrially interesting approaches to 'low-CO₂' cements," *Cem. Concr. Res.*, vol. 34, no. 9, pp. 1489–1498, 2004.
- [8] P. Duxson, A. Fernández-Jiménez, J. L. Provis, G. C. Lukey, A. Palomo, and J. S. J. Van Deventer, "Geopolymer technology: The current state of the art," *J. Mater. Sci.*, vol. 42, no. 9, pp. 2917–2933, 2007.
- [9] M. R. Rowles, J. V. Hanna, K. J. Pike, M. E. Smith, and B. H. O'Connor, "²⁹Si, ²⁷Al, ¹H and ²³Na MAS NMR Study of the Bonding Character in Aluminosilicate Inorganic Polymers," *Appl. Magn. Reson.*, vol. 32, no. 4, pp. 663–689, 2007.
- [10] F. Pacheco-Torgal, J. Labrincha, C. Leonelli, A. Palomo, and P. Chindaprasit, *Handbook of alkali-activated cements, mortars and concretes*. Elsevier, 2014.
- [11] C. Shi, D. Roy, and P. Krivenko, *Alkali-activated cements and concretes*. CRC press, 2003.
- [12] F. Pacheco-Torgal, Z. Abdollahnejad, A. F. Camões, M. Jamshidi, and Y. Ding, "Durability of alkali-activated binders: A clear advantage over Portland cement or an unproven issue?," *Constr. Build. Mater.*, vol. 30, pp. 400–405, 2012.
- [13] J. L. Provis, J. S. J. van Deventer, and S. A. Bernal, *Binder chemistry – Blended systems and intermediate Ca content*, vol. 13. 2014.
- [14] "Geopolymer Cement for mitigation of Global Warming." [Online]. Available: <https://www.geopolymer.org/applications/global-warming/>. [Accessed: 23-Mar-2018].
- [15] P. Duxson, J. L. Provis, G. C. Lukey, and J. S. J. van Deventer, "The role of inorganic polymer technology in the development of 'green concrete,'" *Cem. Concr. Res.*, vol. 37, no. 12, pp. 1590–1597, 2007.

- [16] B. V. Rangan, "Fly Ash-Based Geopolymer Concrete," *Proc. Int. Work. Geopolymer Cem. Concr. December*, vol. 2010, pp. 68–106, 2010.
- [17] I. Lancellotti, E. Kamseu, M. Michelazzi, L. Barbieri, A. Corradi, and C. Leonelli, "Chemical stability of geopolymers containing municipal solid waste incinerator fly ash," *Waste Manag.*, vol. 30, no. 4, pp. 673–679, 2010.
- [18] A. Sathonsaowaphak, P. Chindapasirt, and K. Pimraksa, "Workability and strength of lignite bottom ash geopolymer mortar," *J. Hazard. Mater.*, vol. 168, no. 1, pp. 44–50, Aug. 2009.
- [19] T. W. Cheng and J. P. Chiu, "Fire-resistant geopolymer produce by granulated blast furnace slag," *Miner. Eng.*, vol. 16, no. 3, pp. 205–210, 2003.
- [20] A. Islam, U. J. Alengaram, M. Z. Jumaat, and I. I. Bashar, "The development of compressive strength of ground granulated blast furnace slag-palm oil fuel ash-fly ash based geopolymer mortar," *Mater. Des.*, vol. 56, pp. 833–841, 2014.
- [21] Z. Sun *et al.*, "Synthesis and thermal behavior of geopolymer-type material from waste ceramic," *Constr. Build. Mater.*, vol. 49, pp. 281–287, 2013.
- [22] "Incineration & landfill," vol. 2014, pp. 2014–2015, 2014.
- [23] J. . Chimenos, M. Segarra, M. . Fernández, and F. Espiell, "Characterization of the bottom ash in municipal solid waste incinerator," *J. Hazard. Mater.*, vol. 64, no. 3, pp. 211–222, 1999.
- [24] K. Kahle *et al.*, "Bottom Ash from Wte Plants Metal Recovery and Utilization," pp. 1–30, 2015.
- [25] S. Dugenest, J. Combrisson, H. Casabianca, and M. F. Grenier-Loustalot, "Municipal solid waste incineration bottom ash: Characterization and kinetic studies of organic matter," *Environ. Sci. Technol.*, vol. 33, no. 7, pp. 1110–1115, 1999.
- [26] R. del Valle-Zermeño, "Material characterization of the MSWI bottom ash as a function of particle size. Effects of glass recycling over time," *Sci. Total Environ.*, vol. 581–582, p. 897, 2017.
- [27] "RLG International cementreview."
- [28] J. L. García Sánchez, E. Molina Grima, F. García Camacho, J. a Sánchez Pérez, and D. López Alonso, "(c) Consejo Superior de Investigaciones Científicas Licencia Creative Commons 3.0 España (by-nc) <http://grasasyaceites.revistas.csic.es>," *Grasas Y Aceites*, vol. LIX, no. c, pp. 121–129, 2001.
- [29] A. Miguel, B. Alfonso, D. Natividad, and A. Iglesias, "Ingeniería de materiales," 2014.
- [30] F. A. López, M. C. Pena, and A. López-Delgado, "Hydrolysis and heat treatment of aluminum dust," *J. Air Waste Manag. Assoc.*, vol. 51, no. 6, pp. 903–912, 2001.
- [31] A. López Delgado, J. . Medina, P. Alonso, H. Tayibi, C. Pérez, and F. a. López, "Estudio del comportamiento térmico del polvo de aluminio estabilizado con el yeso," *Rev. Metal.*, vol. 41, no. c, pp. 330–334, 2005.
- [32] D. A. Pereira, B. De Aguiar, F. Castro, M. F. Almeida, and J. A. Labrincha, "Mechanical behaviour of Portland cement mortars with incorporation of Al-containing salt slags," *Cem. Concr. Res.*, vol. 30, no. 7, pp. 1131–1138, 2000.

- [33] A. López-delgado, H. Tayibi, C. Pérez, and F. J. Alguacil, "A hazardous waste from secondary aluminium metallurgy as a new raw material for calcium aluminate glasses."
- [34] J. Javier, V. Rodríguez, A. M. Murciego, N. A. Iglesias, J. Diego, and F. Silva, "Preparation and Characterization of Materials Obtained from Concrete and Paval Wastes," pp. 145–146, 2015.
- [35] A. Kumar and S. Kumar, "Development of paving blocks from synergistic use of red mud and fly ash using geopolymerization," *Constr. Build. Mater.*, vol. 38, pp. 865–871, 2013.
- [36] W. Hajjaji *et al.*, "Composition and technological properties of geopolymers based on metakaolin and red mud," *Mater. Des.*, vol. 52, pp. 648–654, 2013.
- [37] N. Ye *et al.*, "Synthesis and characterization of geopolymer from bayer red mud with thermal pretreatment," *J. Am. Ceram. Soc.*, vol. 97, no. 5, pp. 1652–1660, 2014.
- [38] A. Gil and S. A. Korili, "Management and valorization of aluminum saline slags: Current status and future trends," *Chem. Eng. J.*, vol. 289, pp. 74–84, 2016.
- [39] E. Alakangas, "Quality guidelines of wood fuels in Finland VTT-M-04712-15." 2015.
- [40] C. Ruiz-Santaquiteria, a Fernández-Jiménez, and a Palomo, "Quantitative determination of reactive SiO₂ and Al₂O₃ in aluminosilicate materials," *13th Int. Congr. Chem. Cem.*, pp. 1–7, 2011.
- [41] "Hernández-Gutiérrez, L.E., Santamarta, J.C., Tomás, R., Cano, M., García-Barba, J., Piñero-García, A. (2013). Prácticas de Ingeniería del Terreno. Universidades de Alicante y de La Laguna. <http://web.ua.es/es/ginter/> ó <http://ocw.uil.es/> (23/05/2018)," 2007.
- [42] "Waste Acceptance Criteria - Overview," vol. 44, no. WSC-WAC-OVR V 2.0, p. 2003, 2017.
- [43] S. Hanjitsuwan, S. Hunpratub, P. Thongbai, S. Maensiri, V. Sata, and P. Chindaprasirt, "Effects of NaOH concentrations on physical and electrical properties of high calcium fly ash geopolymer paste," *Cem. Concr. Compos.*, vol. 45, pp. 9–14, 2014.
- [44] S. Pangdaeng, T. Phoo-ngernkham, V. Sata, and P. Chindaprasirt, "Influence of curing conditions on properties of high calcium fly ash geopolymer containing Portland cement as additive," *Mater. Des.*, vol. 53, pp. 269–274, 2014.
- [45] E. Ul Haq, S. Kunjalukkal Padmanabhan, and A. Licciulli, "Synthesis and characteristics of fly ash and bottom ash based geopolymers-A comparative study," *Ceram. Int.*, vol. 40, no. 2, pp. 2965–2971, 2014.
- [46] K. Djebaili, Z. Mekhalif, A. Boumaza, and A. Djelloul, "XPS, FTIR, EDX, and XRD Analysis of Al₂O₃ Scales Grown on PM2000 Alloy," vol. 2015, pp. 1–14, 2013.
- [47] H. Xu, Q. Li, L. Shen, W. Wang, and J. Zhai, "Synthesis of thermostable geopolymer from circulating fluidized bed combustion (CFBC) bottom ashes," *J. Hazard. Mater.*, vol. 175, no. 1–3, pp. 198–204, 2010.
- [48] K. Boonserm, V. Sata, K. Pimraksa, and P. Chindaprasirt, "Improved geopolymerization of bottom ash by incorporating fly ash and using waste gypsum as additive," *Cem. Concr. Compos.*, vol. 34, no. 7, pp. 819–824, 2012.

APPENDICES

8. APPENDIX 1: GLOSSARY

AAC	Alkali Activated Cement
BA	Bottom Ash
BSD	Backscattered electron Detector
CCiTUB	Centres Científics i Tècnics de la Universitat de Barcelona
EDS	Energy Dispersive X-Ray Spectrometry
ETD	Everhart Thornley Detector
EU	European Union
FA	Fly Ash
FTIR	Fourier-Transform Infrared Spectroscopy
ICP-MS	Inductively Coupled Plasma - Mass Spectrometry
ICP-OES	Inductively Coupled Plasma – Optical Emission Spectrometry
LCA	Life Cycle Analysis
LOI	Loss on Ignition
MSWI BA	Municipal Solid Waste Incineration Bottom Ash
PSD	Particle Size Distribution
SEM	Scanning Electron Microscopy
SIRUSA	Servei d'Incineració de Residus Sòlids Urbans, SA
VECSA	Valorización de Escorias de la Combustión, SA
WBA	Weathered Bottom Ash
XRD	X-Ray Diffraction
XRF	X-Ray Fluorescence

9. APPENDIX 2: ECONOMIC EVALUATION

In this appendix, the total cost of the project is calculated: the raw materials cost, equipment and services used, staff and non-reusable material.

Table 8: Raw materials cost

Material	kg	€/kg	€
NaOH	0,3	34,44	10,33
Na ₂ SiO ₃	0,75	3,86 (9,26 €/l)	2,90
BA	35,4	0	0
Paval	0,4	0	0
Total	-	-	13,23

Table 9: Services and equipment cost

Service	H	€/h	€
Grind	3	10,20	20,40
Mill	20 (39 times mill)	0,67 €/mill	26,31
Sieve	7	8,96	62,72
PSD	2	29,29	59,8
XRF	1	25,24	25,24
XRD	2	10,20	20,40
FTIR	4	21,72	86,88
SEM	7	19,06	133,42
EDS	7	8,60	60,20
ICP-MS	2	45,87	91,74

ICP-OES	1	44,08	44,08
Total	-	-	631,19

Table 10: Staff cost

Activity	h	€/h	€
Laboratory	260	8	2080
Bibliographic research	50	8	400
Project redaction	100	8	800
Tutor	120	12	1440
Total	-	-	4720

Table 11: Non-reusable material cost

Material	€
Non-reusable material	75

The total cost of the project is approximately 5439,42 €.

10. APPENDIX 3: RAW MATERIALS PSD

PSD (in mass %) of BA and Paval without treatment, performed by sieving the materials and weighting every fraction. It can be seen in Figure 48 that the amount of coarse particles is lower than the amount of fine particles.

In Paval, it can be seen in Figure 49 that an important amount of sample has particle size lower than 80 μm without being treated, which will reduce the time in sample preparation.

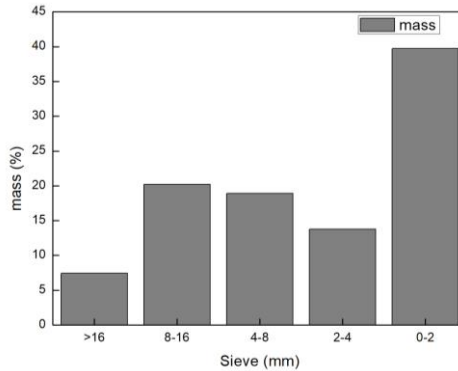


Figure 48: BA PSD

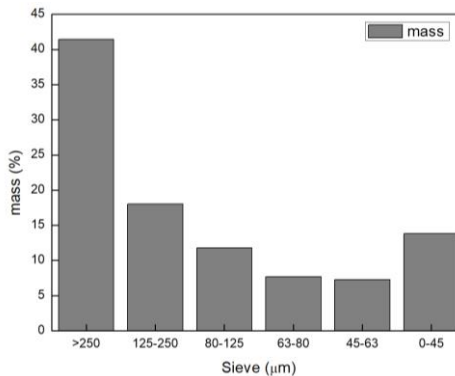


Figure 49: Paval PSD

11. APPENDIX 4: MASS AND VOLUME VARIATION

In this appendix, graphs of mass variation and volume contraction are presented.

11.1 TEST SAMPLES 3

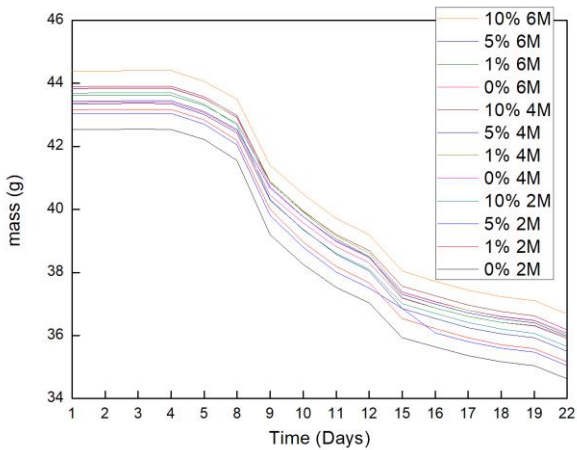


Figure 50: Mass variation in test samples 3

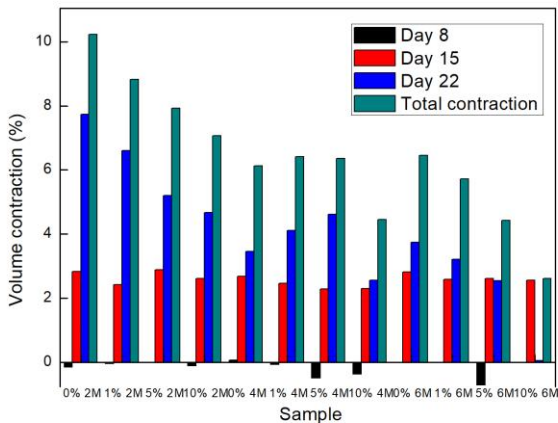


Figure 51: Volume contraction in test samples 3

11.2 DEFINITIVE SAMPLES

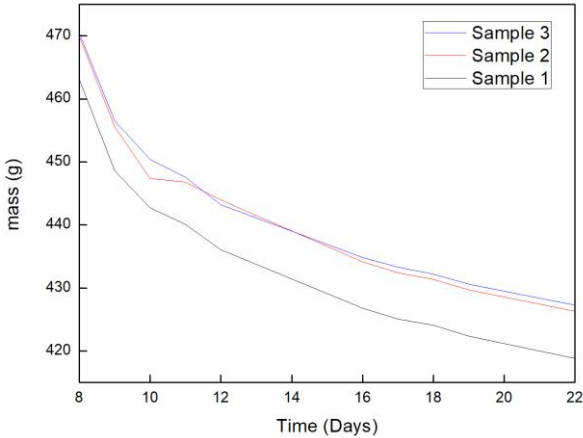


Figure 52: Mass change in definitive samples

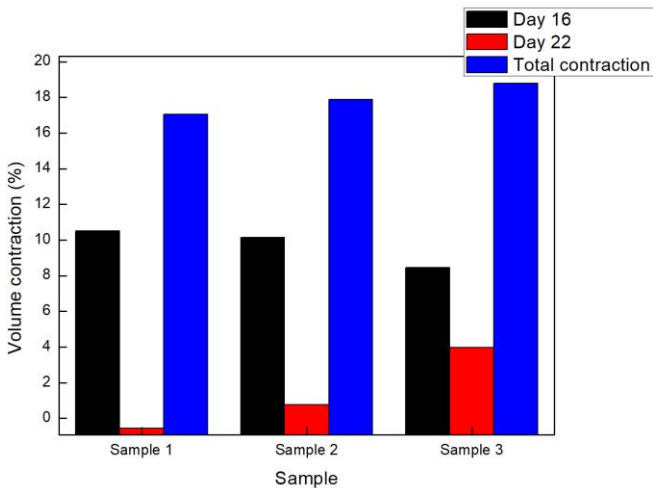


Figure 53: Volume contraction in definitive samples

In Figure 52 and Figure 53 there is only values since day 8, as the days before the samples were all in the same mold so they cannot be treated separately.

12. APPENDIX 5: PAVAL MOISTURE DETERMINATION

1g of Paval was weighted before and after 24h in an oven at 105 °C per duplicate, and the % of moisture was calculated with Eq.7, where W_M is wet mass and D_M is dry mass.

$$\% \text{ Moisture} = \frac{W_M - D_M}{D_M} \cdot 100 \quad (7)$$

Table 12: Paval moisture determination results

Sample	Initial mass (W_M)	Final mass (W_D)	% moisture
Paval 1	0,998	0,997	0,1%
Paval 2	1,001	1,000	0,1%

With these results we can conclude that the Paval sample used had no moisture, because this 0,001 g can be the error of the scale.

13. APPENDIX 6: LEACHING TEST RESULTS

In this appendix the leaching test table explained in 5.1.4 are presented.

Table 13: Raw materials ICP-MS leaching test results

Sample	Zn (mg/kg)	Pb (mg/kg)	Ni (mg/kg)	Cr (mg/kg)	Cu (mg/kg)	Ba (mg/kg)
Paval average	0,21	0,02	<0.2	0,06	0,21	0,06
BA>8 mm (unmilled) average	0,20	0,04	<0.2	0,04	0,85	0,18
BA>8 mm (milled) average	0,26	0,16	<0.2	0,05	1,54	0,18
Inert limit	4	0,5	0,4	0,5	2	20
Non-hazardous	50	10	10	10	50	100
Hazardous limit	200	50	40	70	100	300

Sample	As (mg/kg)	Cd (mg/kg)	Sb (mg/kg)	Mo (mg/kg)	Hg (mg/kg)
Paval average	0,04	0,01	0,84	8,59	0,15
BA>8 mm (unmilled) average	0,00	0,00	0,17	0,31	0,05
BA>8 mm (milled) average	0,01	0,00	0,33	0,28	0,07
Inert limit	0,5	0,04	0,06	0,5	0,01
Non-hazardous	2	1	0,7	10	0,2
Hazardous limit	25	5	5	30	2

14. APPENDIX 7: XRD RESULTS

In this appendix, XRD graphs of test samples 3 samples are presented

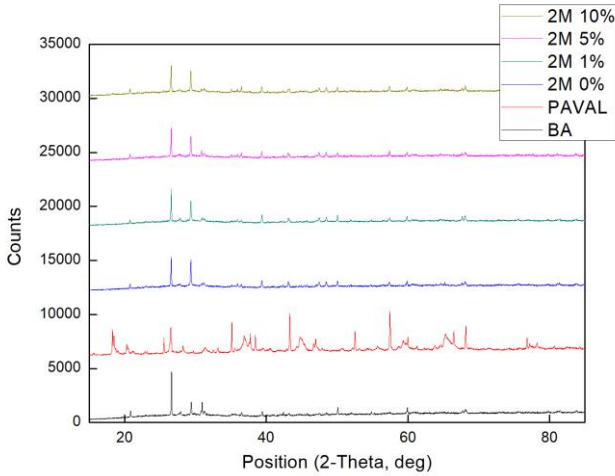


Figure 54: XRD NaOH 2M test samples 3

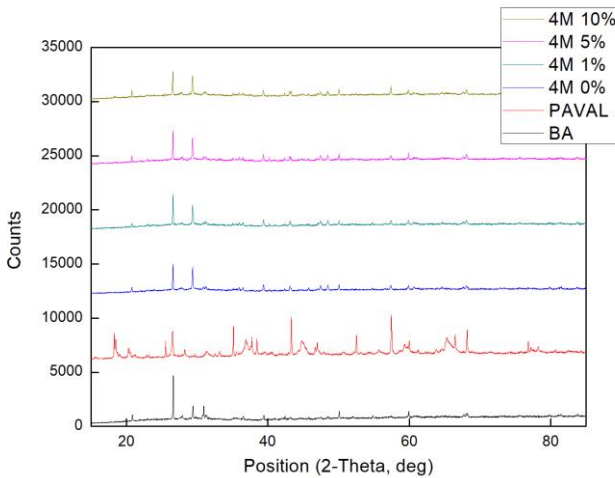


Figure 55: XRD NaOH 4M test samples 3

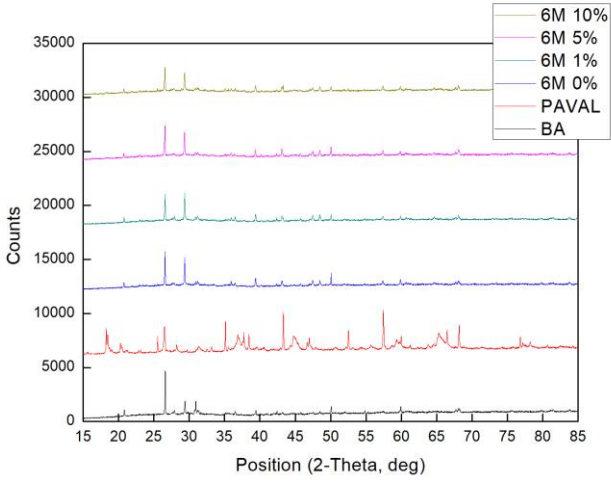


Figure 56: XRD NaOH 6M test samples 3

15. APPENDIX 8: FTIR RESULTS

In this appendix, FTIR graphs of test samples 3 samples are presented.

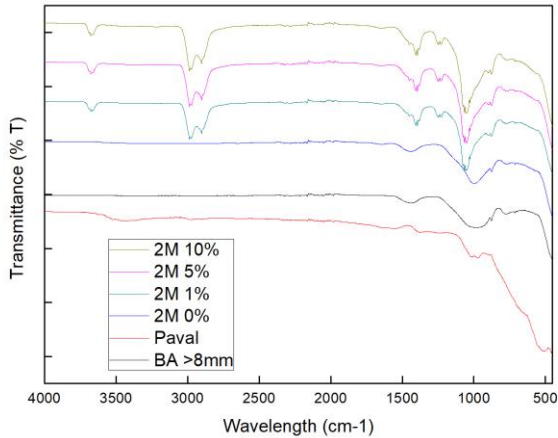


Figure 57: FTIR of NaOH 2M test samples 3

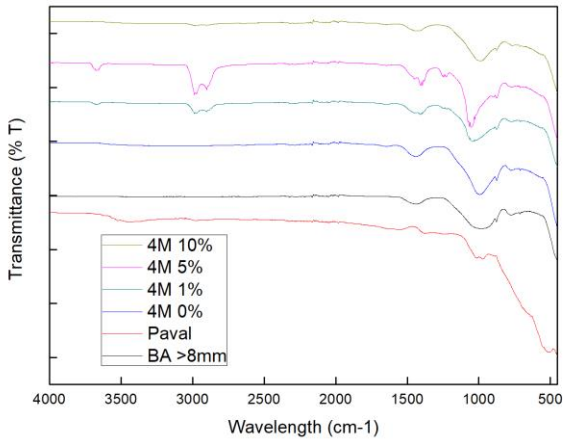


Figure 58: FTIR of NaOH 4M test samples 3

16. APPENDIX 9: RAW MATERIALS SEM AND EDS

In this appendix, SEM images and EDS of the spots of raw materials are presented.

16.1 BA SEM IMAGES

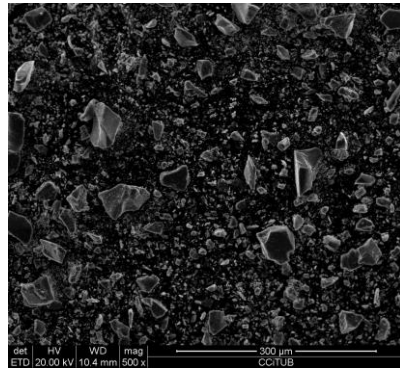
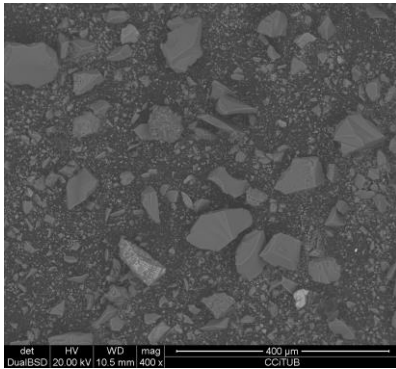


Figure 59: BA BSD 400x (a) BA ETD 500x (b)

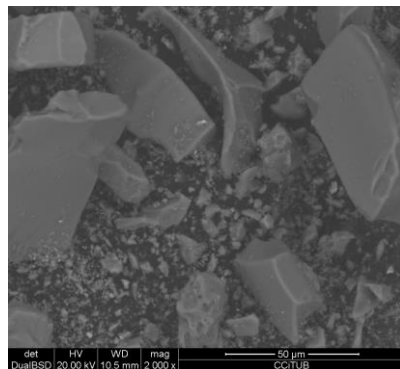
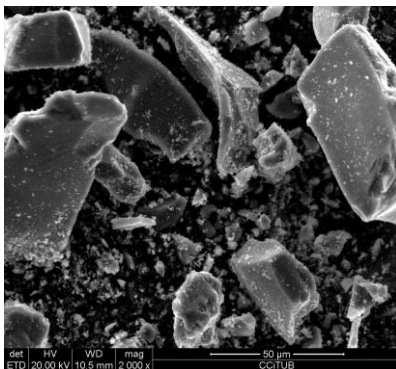


Figure 60: BA ETD 2000x (a) BA BSD 2000x (b)

16.2BA EDS

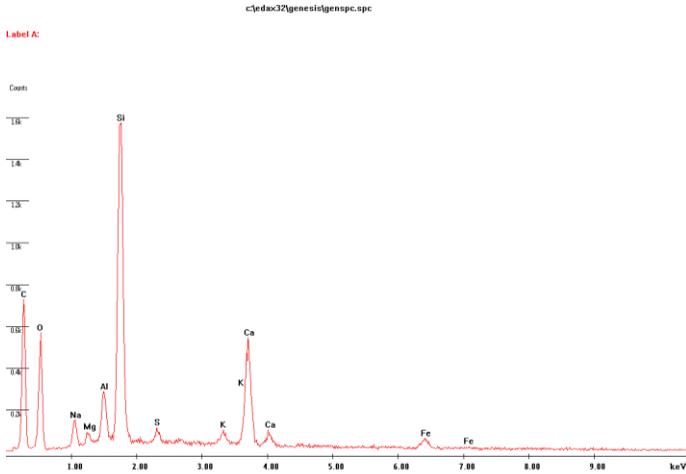


Figure 61: BA full frame EDS

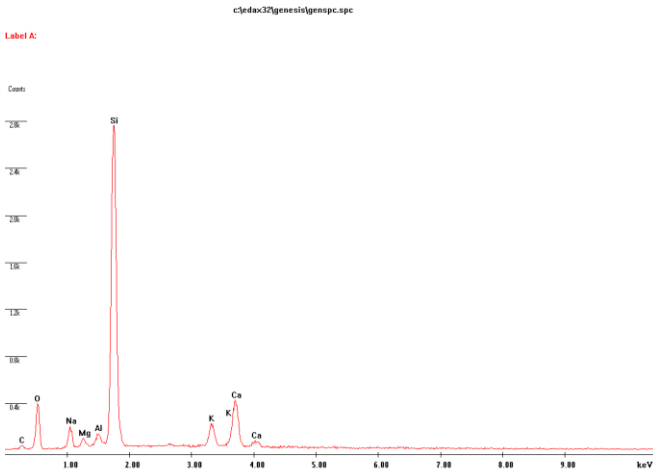


Figure 62: BA spot 1 EDS

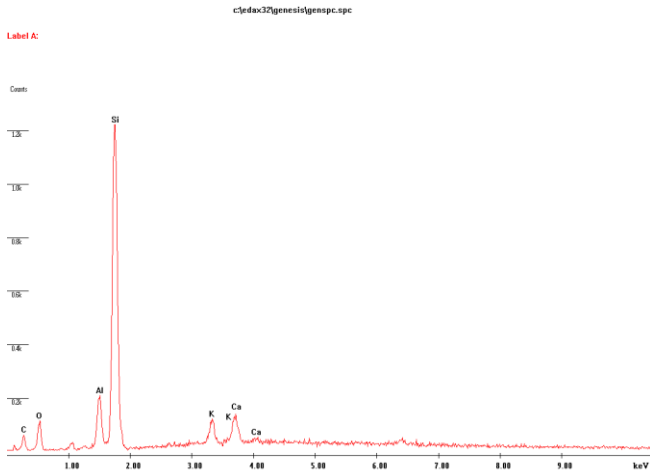


Figure 63: BA spot 2 EDS

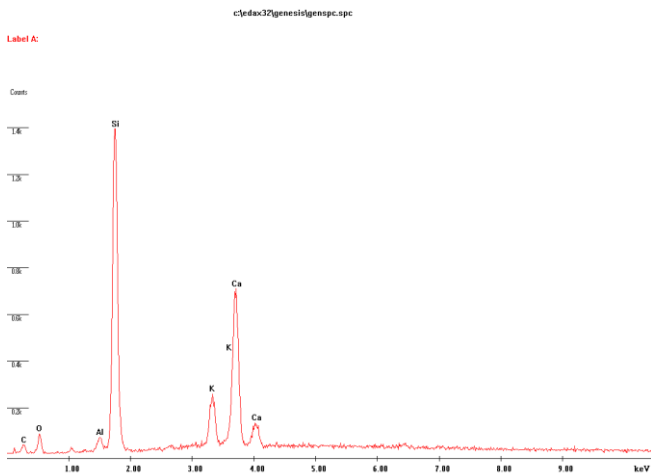


Figure 64: BA spot 3 EDS

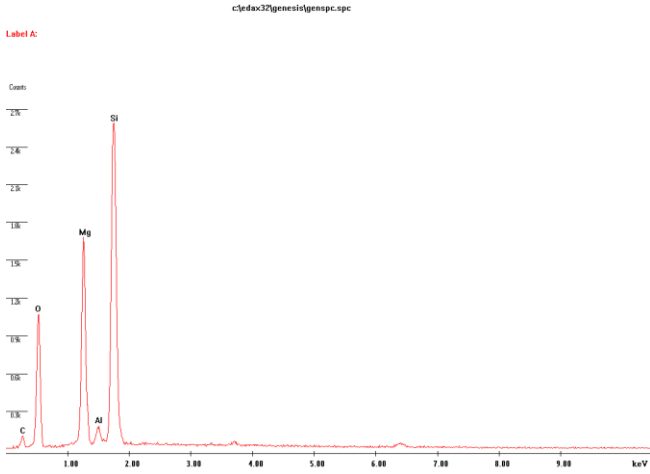


Figure 65: BA spot 4 EDS

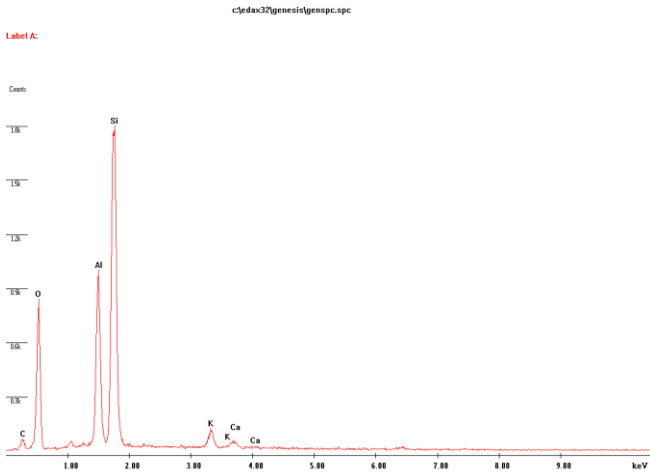


Figure 66: BA spot 5 EDS

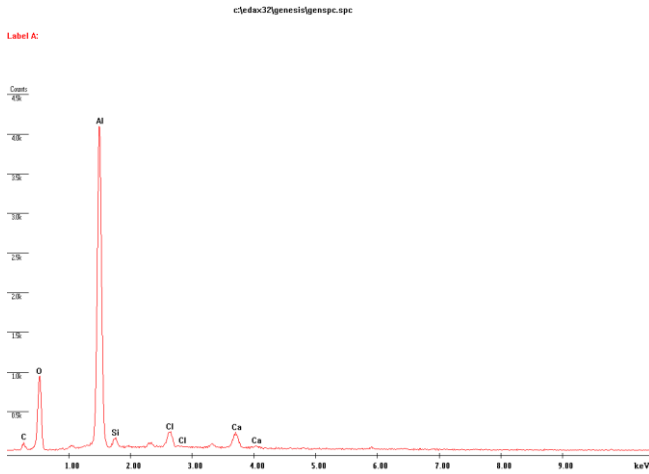


Figure 67: BA spot 6 EDS

16.3 PAVAL SEM IMAGES

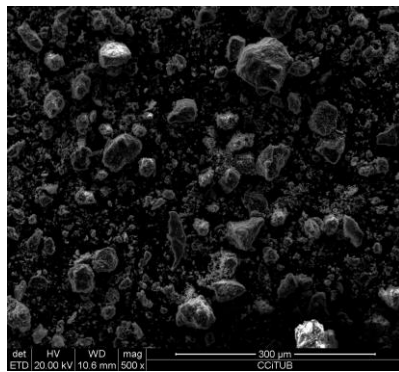
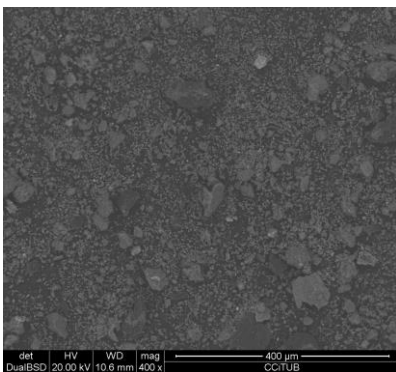


Figure 68: Paval BSD 400x (a) Paval ETD 500x (b)

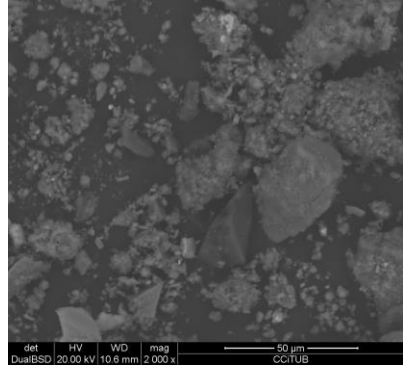
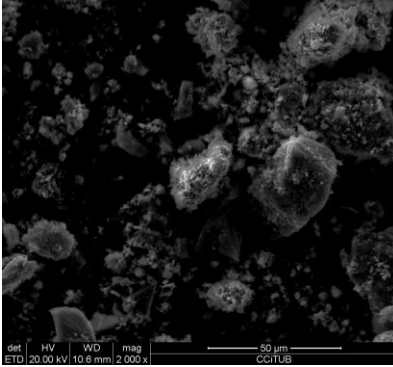


Figure 69: Paval ETD 2000x (a) Paval BSD 2000x (b)

16.4PAVAL EDS

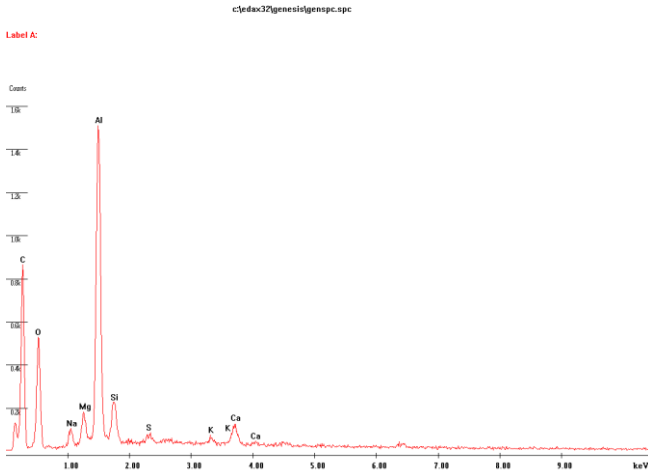


Figure 70: Paval full frame EDS

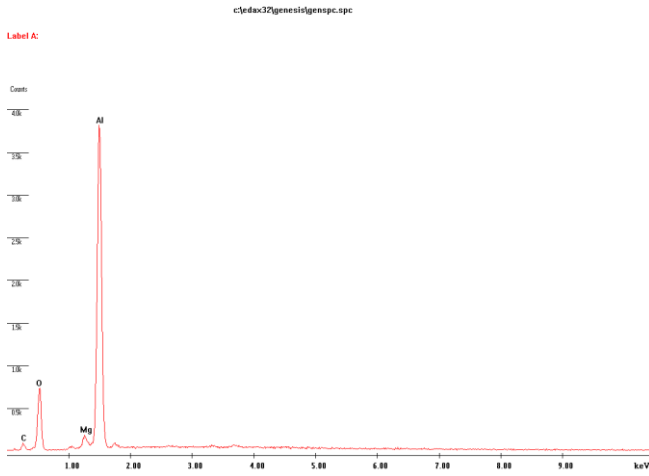


Figure 71: Paval spot 1 EDS

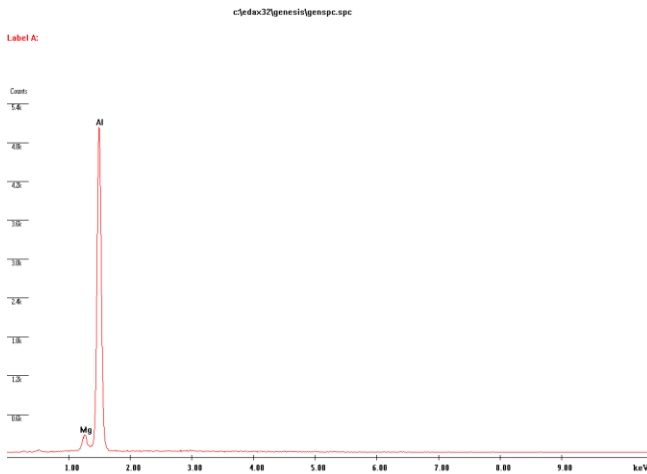


Figure 72: Paval spot 2 EDS

17. APPENDIX 10: TEST SAMPLES 3 SEM

In this appendix, SEM images and EDS of the spots of test samples 3 are presented.

17.1 NaOH 2M SAMPLES

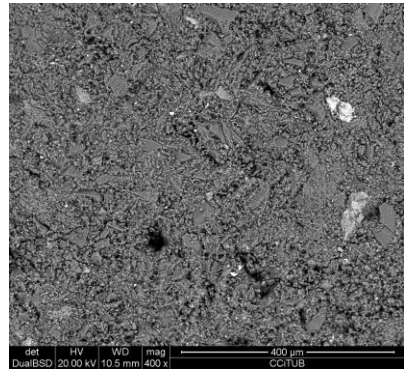
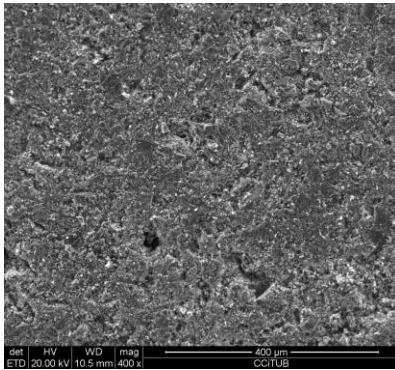


Figure 73: 0% 2M ETD 400x (a) 0% 2M BSD 400x (b)

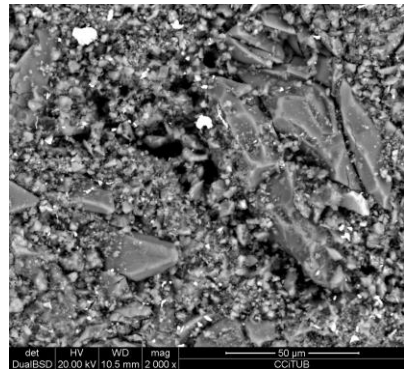
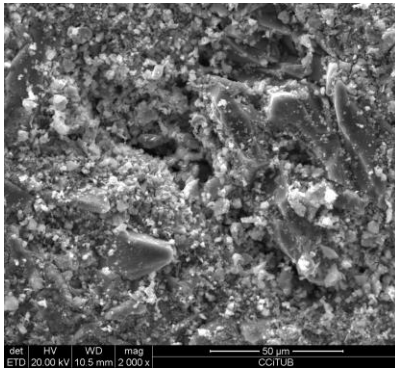


Figure 74: 0% 2M ETD 2000x (a) 0% 2M BSD 2000x (b)

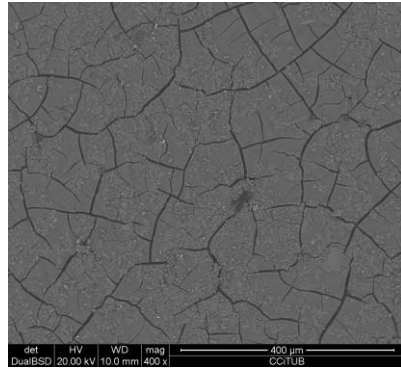
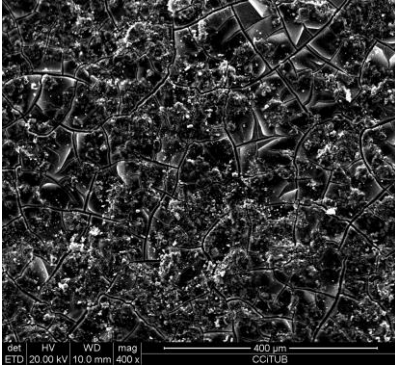


Figure 75: 1% 2M ETD 400x (a) 1% 2M BSD 400x (b)

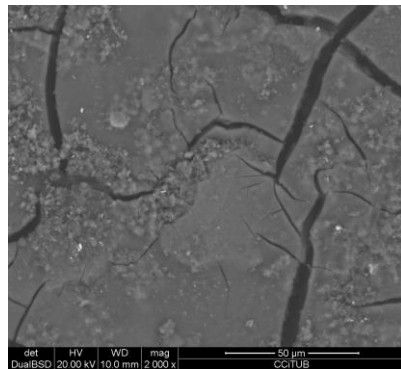
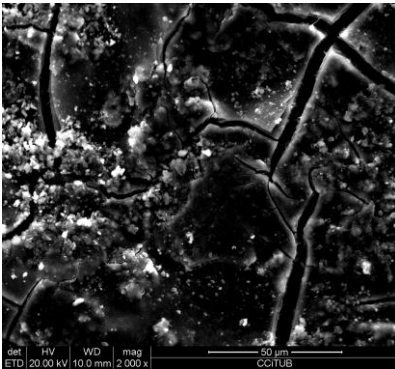


Figure 76: 1% 2M ETD 2000x (a) 1% 2M BSD 2000x (b)

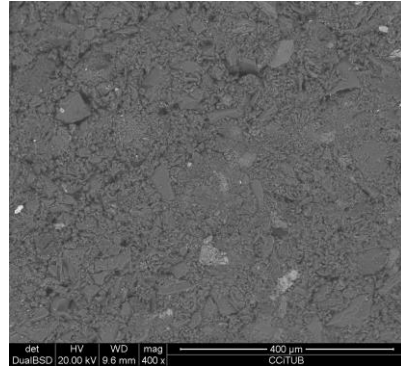
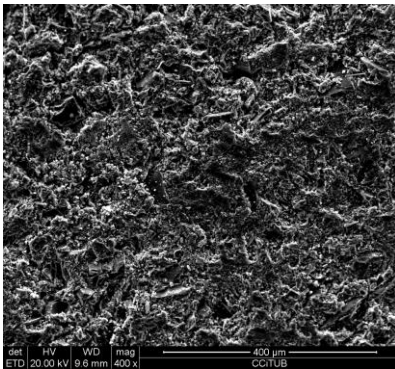


Figure 77: 5% 2M ETD 400x (a) 5% 2M BSD 400x (b)

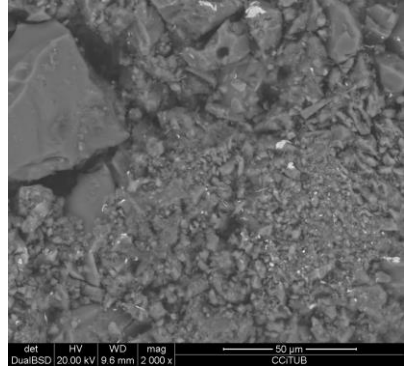
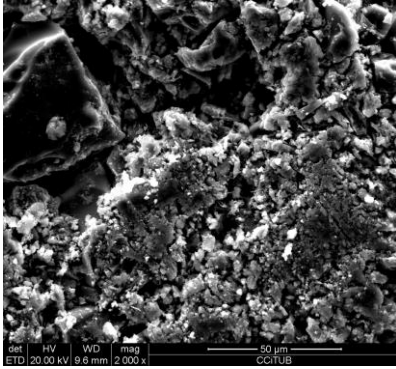


Figure 78: 5% 2M ETD 2000x (a) 5% 2M BSD 2000x (b)

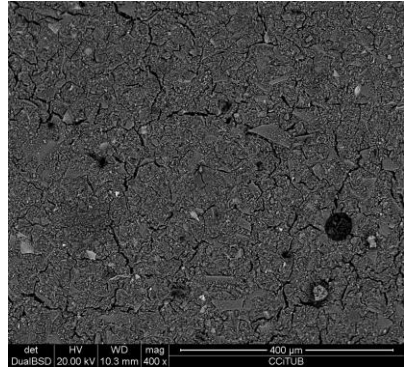
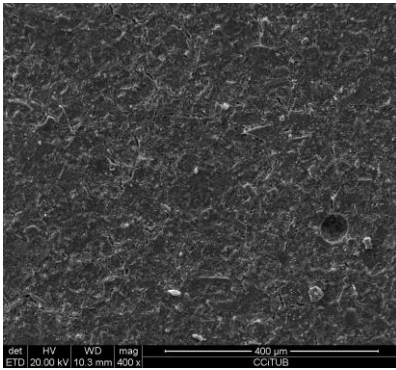


Figure 79: 10% 2M ETD 400x (a) 10% 2M BSD 400x (b)

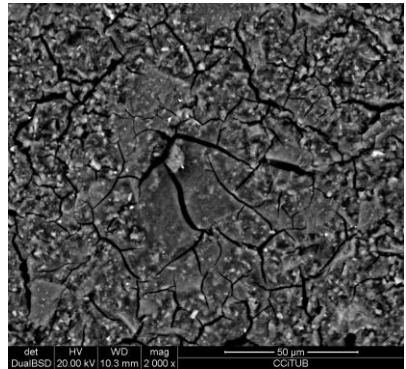
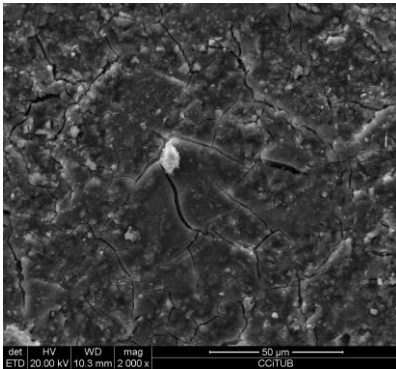


Figure 80: 10% 2M ETD 2000x (a) 10% 2M BSD 2000x (b)

17.2NAOH 4M SAMPLES

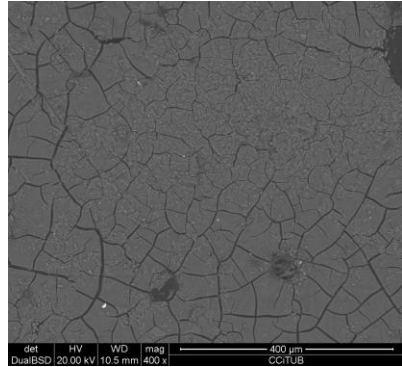
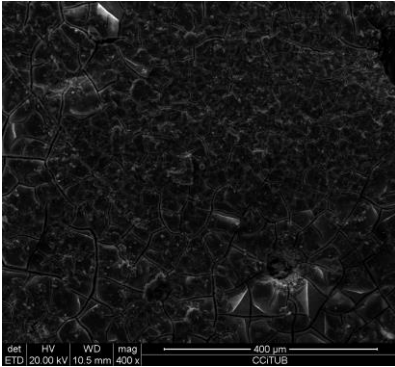


Figure 81: 0% 4M ETD 400x (a) 0% 4M BSD 400x (b)

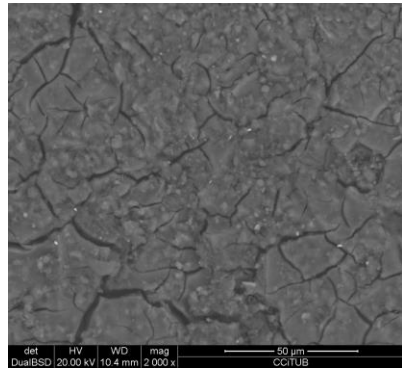
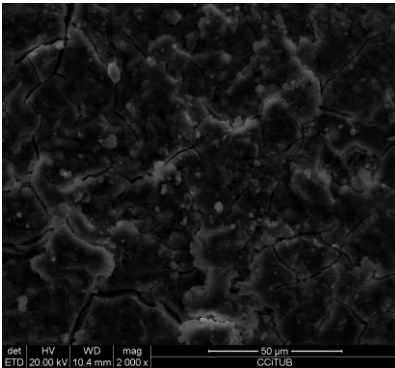


Figure 82: 0% 4M ETD 2000x (a) 0% 4M BSD 2000x (b)

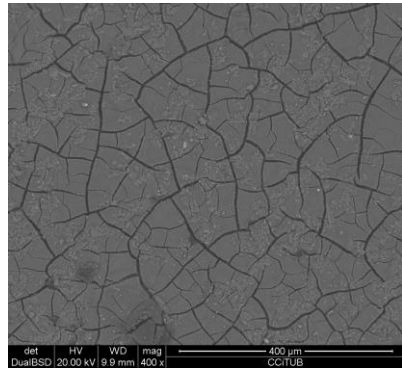
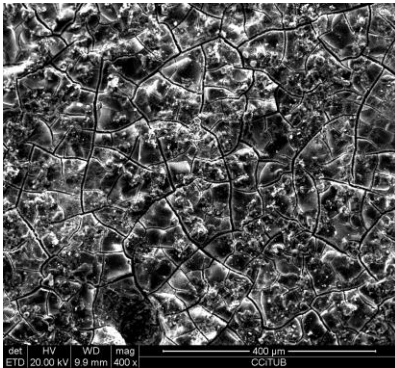


Figure 83: 1% 4M ETD 400x (a) 1% 4M BSD 400x (b)

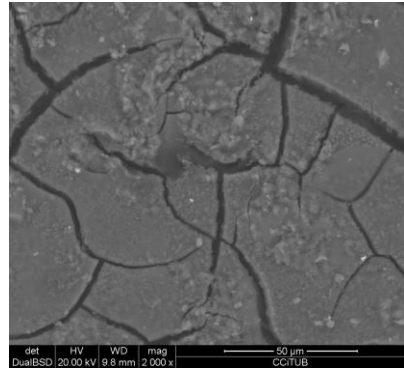
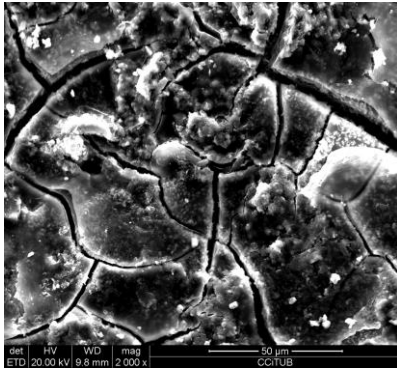


Figure 84: 1% 4M ETD 2000x (a) 1% 4M BSD 2000x (b)

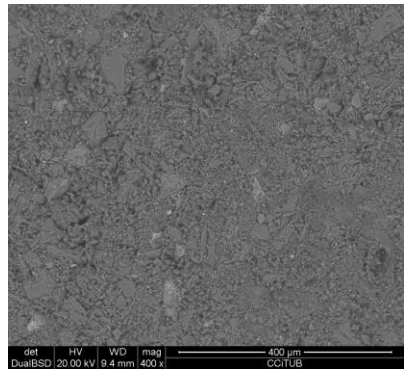
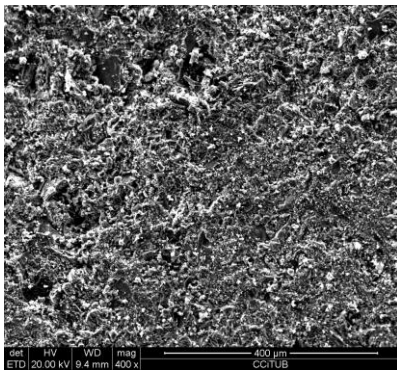


Figure 85: 5% 4M ETD 400x (a) 5% 4M BSD 400x (b)

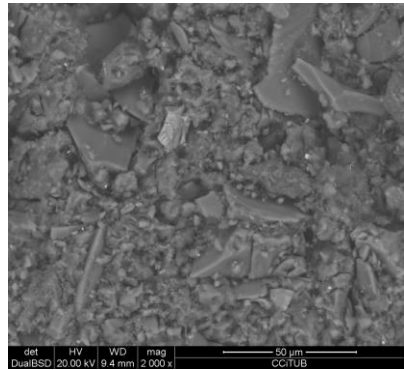
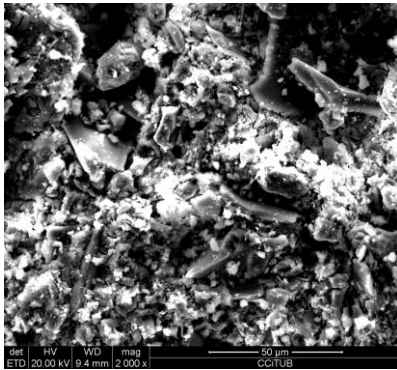


Figure 86: 5% 4M ETD 2000x (a) 5% 4M BSD 2000x (b)

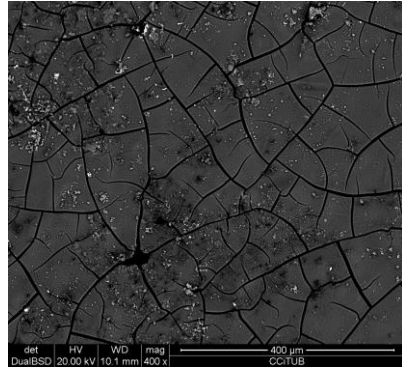
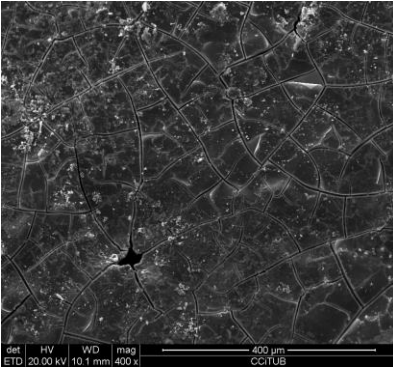


Figure 87: 10% 4M ETD 400x (a) 10% 4M BSD 400x (b)

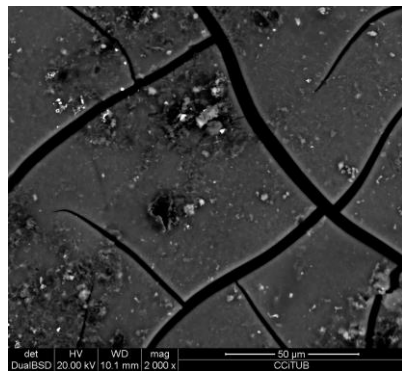
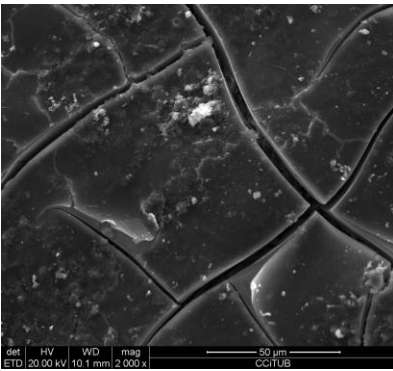


Figure 88: 10% 4M ETD 2000x (a) 10% 4M BSD 2000x (b)

17.3NAOH 6M SAMPLES

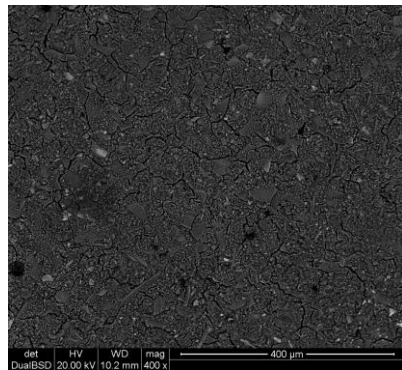
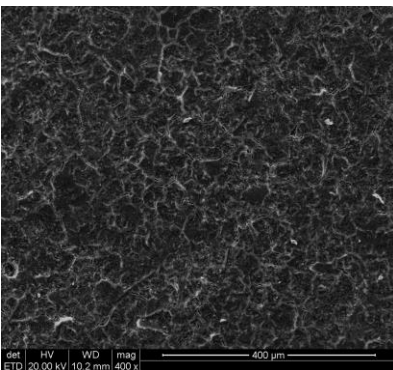


Figure 89: 0% 6M ETD 400x (a) 0% 6M BSD 400x (b)

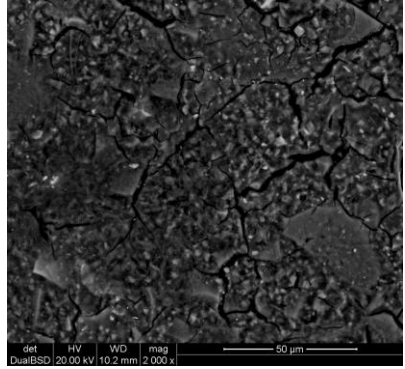
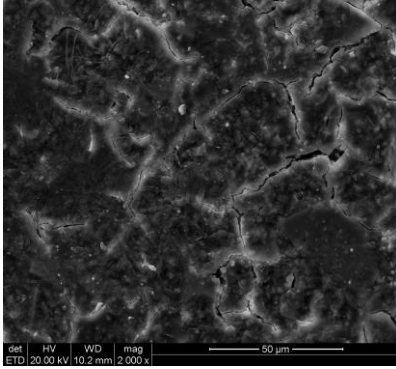


Figure 90: 0% 6M EDS 2000x (a) 0% 6M BSD 2000x (b)

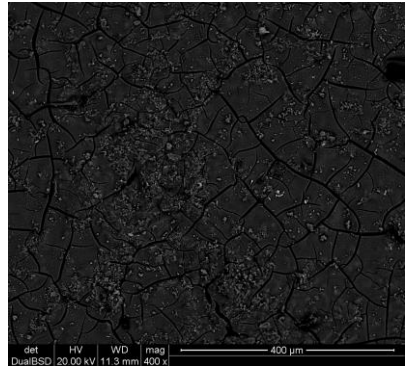
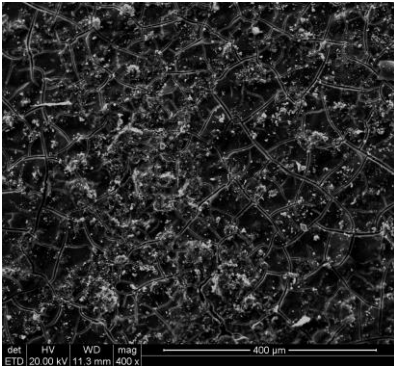


Figure 91: 1% 6M EDS 400x (a) 1% 6M BSD 400x (b)

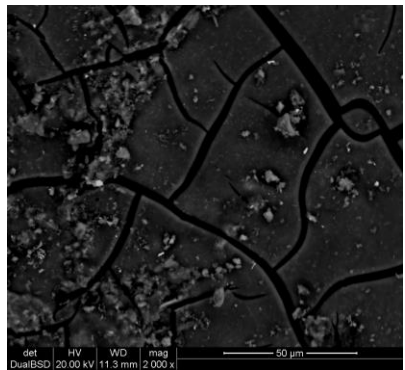
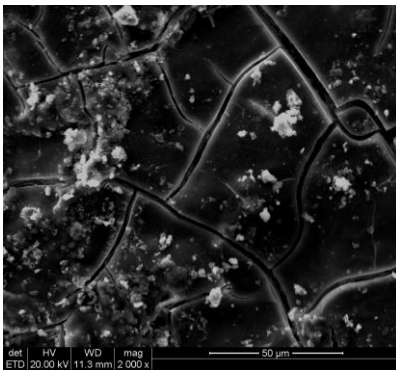


Figure 92: 1% 6M ETD 2000x (a) 1% 6M BSD (b)

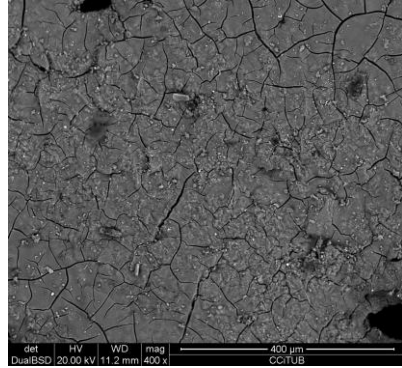
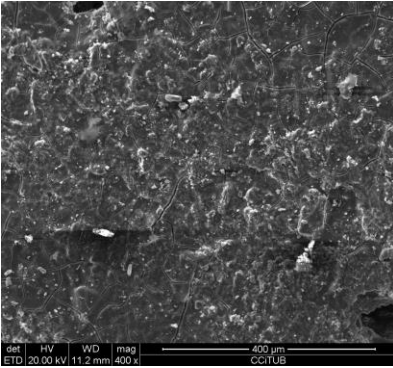


Figure 93: 5% 6M ETD 400x (a) 5% 6M BSD 400x (b)

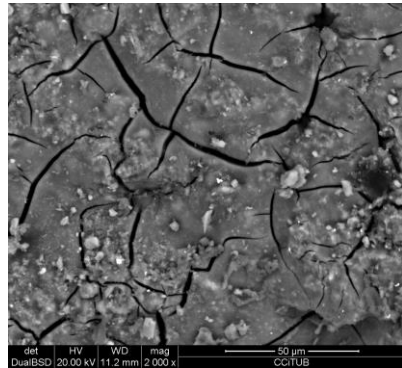
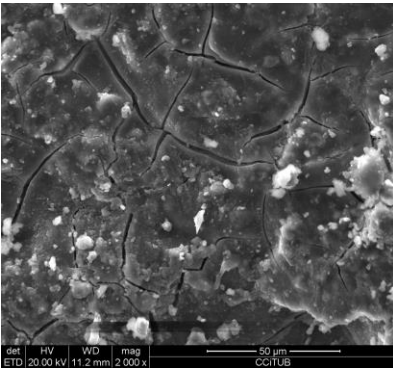


Figure 94: 5% 6M ETD 2000x (a) 5% 6M BSD 2000x (b)

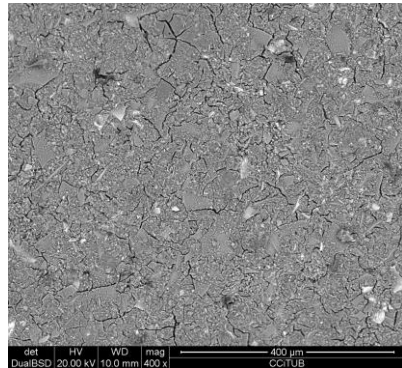
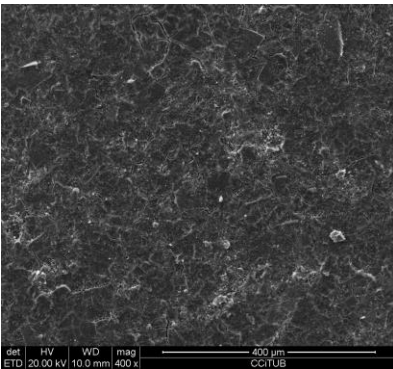


Figure 95: 10% 6M ETD 400x (a) 10% 6M BSD 400x (b)

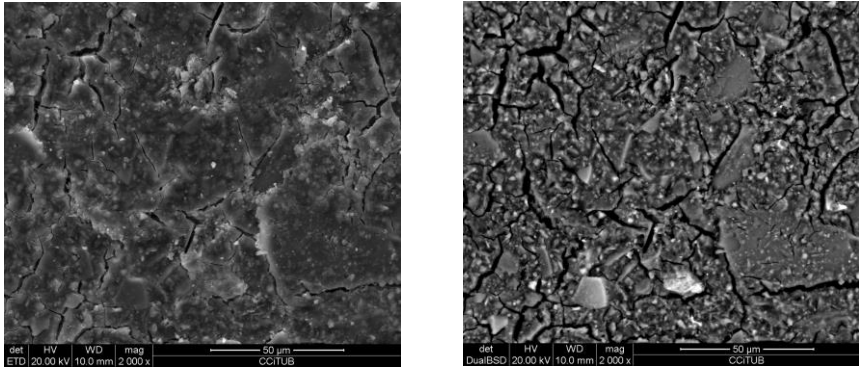


Figure 96: 10% 6M ETD 2000x (a) 10% 6M BSD 2000x (b)

18. APPENDIX 11: DEFINITIVE SAMPLE SEM, EDS AND QUANTITATIVE ANALYSIS

In this appendix, SEM images, EDS of the spots and their correspondent quantitative analysis of the definitive sample are presented.

18.1 DEFINITIVE SAMPLE SEM IMAGES

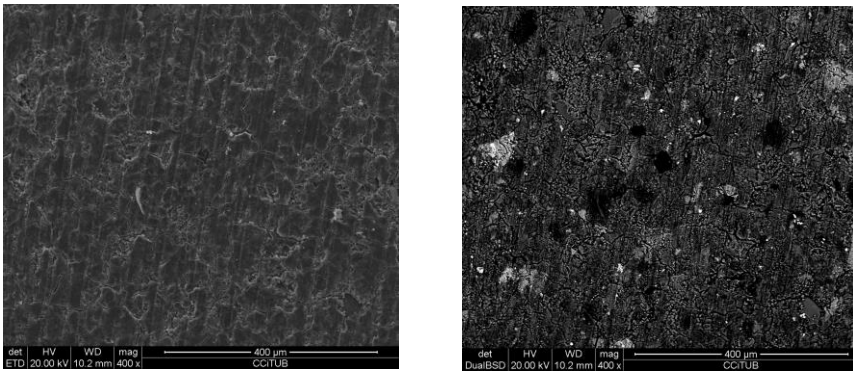


Figure 97: Definitive sample EDS 400x (a) Definitive sample BSD 400x (b)

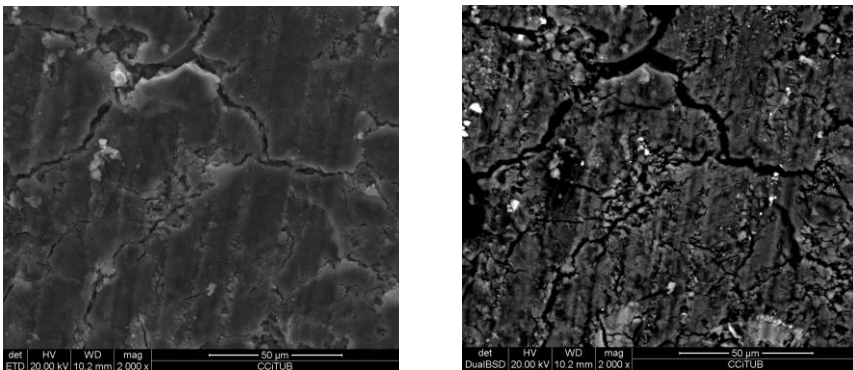


Figure 98: Definitive sample ETD 2000x (a) Definitive sample BSD 2000x (b)

18.2 DEFINITIVE SAMPLES EDS

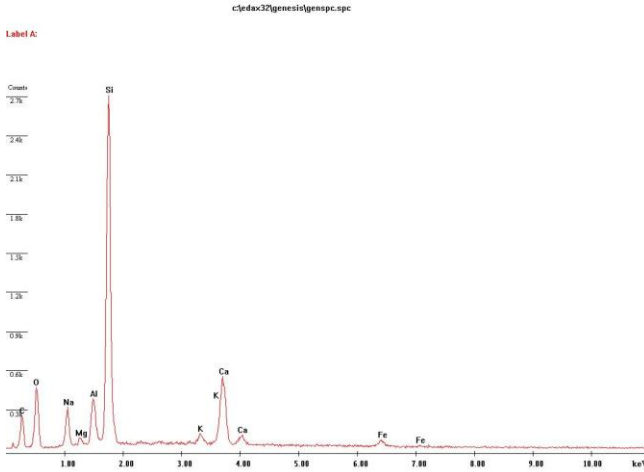


Figure 99: Definitive sample full frame EDS

Table 14: Definitive sample full frame quantitative analysis

Element	Wt (%)
C K	29,1
O K	20,15
Na K	4,28
Mg K	0,66
Al K	3,72
Si K	28,53
K K	1,21
Ca K	9,86
Fe K	2,5
Total	100

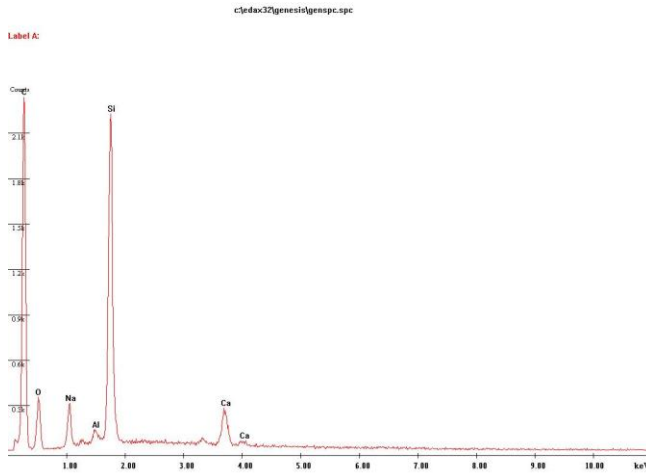


Figure 100: Definitive sample spot 1 EDS

Table 15: Definitive sample spot 1 quantitative analysis

Element	Wt %
C K	74,3
O K	9,35
Na K	1,99
Al K	0,5
Si K	11,5
Ca K	2,37
Total	100

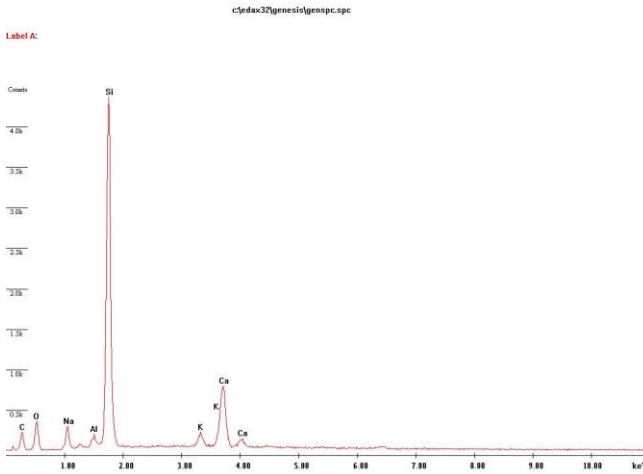


Figure 101: Definitive sample spot 2 EDS

Table 16: Definitive sample spot 2 quantitative analysis

Element	Wt (%)
C K	26,16
O K	14,75
Na K	3,36
Al K	1,25
Si K	38,58
K K	2,49
Ca K	13,41
Total	100

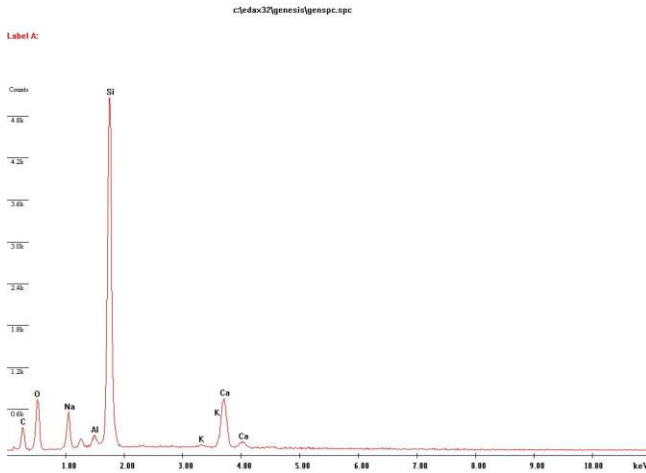


Figure 102: Definitive sample spot 3 EDS

Table 17: Definitive sample spot 3 quantitative analysis

Element	Wt (%)
C K	27,41
O K	21,46
Na K	4,79
Al K	1,17
Si K	35,2
K K	0,49
Ca K	9,48
Total	100

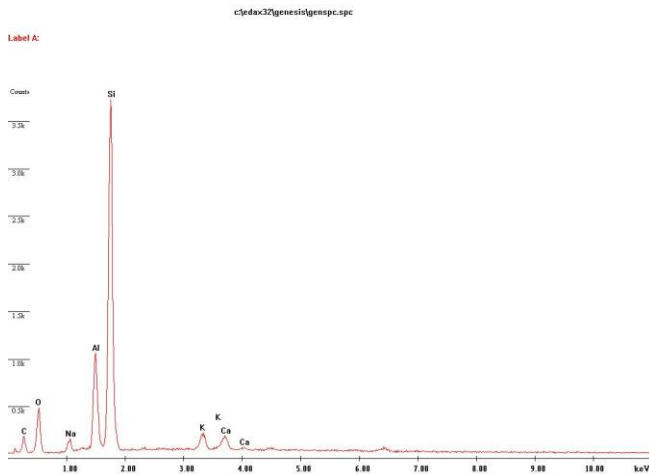


Figure 103: Definitive sample spot 4 EDS

Table 18: Definitive sample spot 4 quantitative analysis

Element	Wt (%)
C K	24,29
O K	18,59
Na K	1,61
Al K	9,21
Si K	40,07
K K	3,22
Ca K	3,02
Total	100